Available online at www.sciencedirect.com

ScienceDirect

www.elsevier.com/locate/jmbbm

Research Paper

One-dimensional nonlinear elastodynamic models and their local conservation laws with applications to biological membranes

A.F. Cheviakov[a,*], J.-F. Ganghoffer[b]

[a]Department of Mathematics and Statistics, University of Saskatchewan, Canada
[b]LEMTA - ENSEM, Université de Lorraine, Nancy, France

ARTICLE INFO

Article history:
Received 16 June 2015
Received in revised form
11 August 2015
Accepted 17 August 2015
Available online 28 August 2015

Keywords:
Biological membranes
Nonlinear wave equations
Conservation laws
Fiber-reinforced materials
Hyperelasticity
Viscoelasticity

ABSTRACT

The framework of incompressible nonlinear hyperelasticity and viscoelasticity is applied to the derivation of one-dimensional models of nonlinear wave propagation in fiber-reinforced elastic solids. Equivalence transformations are used to simplify the resulting wave equations and to reduce the number of parameters. Local conservation laws and global conserved quantities of the models are systematically computed and discussed, along with other related mathematical properties. Sample numerical solutions are presented. The models considered in the paper are appropriate for the mathematical description of certain aspects of the behavior of biological membranes and similar structures.

1. Introduction

Biological membranes are thin soft biological structures that play vital roles in a living organism (Humphrey, 1998), and optimize their shape and function in response to stimuli from the environment (Badir et al., 2013; Checa et al., 2011). With their thickness rarely exceeding a few millimeters, biomembranes are able to withstand large physiological loads. Typical examples of biomembranes include the skin (Zöllner et al., 2012), the mucous membrane lining the air–organ interfaces of the respiratory and digestive systems (Li et al., 2011), the fetal membrane (Joyce et al., 2009), the tympanic membrane (Fay et al., 2005), and the heart valve membranes (Rabbah et al., 2013).

The membrane of a biological cell involves an assembly of filaments linked together as a part of a network, or associated with the cell membrane to build a two-dimensional thin sheet. Two-dimensional biological networks may be wrapped around a cell as its wall, or attached to its plasma or nuclear membrane. Structural elements of biological cells are soft and responsible for the large deformability and easy motion of the cell, contrary to majority of the engineered man-made thin structural materials used in sheet industries. The mechanics of biological membranes is clearly related to the network architecture and the elasticity of the filaments. Mechanical models for cells can be derived using either micro/nanostructural or continuum approaches, as explained in detail, for

*Corresponding author.
E-mail address: shevyakov@math.usask.ca (A.F. Cheviakov).

http://dx.doi.org/10.1016/j.jmbbm.2015.08.027
1751-6161/

example, in Assidi et al. (2011) and references therein. Although the continuum approach is more straightforward, the identification of the continuum behavior of a membrane is challenging, as the membrane may be highly anisotropic due to unequal chain lengths and properties of the threads. The constitution of biomembranes as bilayers entails a rather floppy behavior, with bending as the dominant deformation mode in comparison to stretching (Boal, 2012).

The complex mechanical behavior of soft biological tissues results from the deformations and interactions of the constituent phases, including collagen, elastin, muscular, and matrix components, such as proteoglycans. Collagen fibre-rich tissues are classically modeled as composite materials made of one or several families of collagen fibers immersed into a very soft isotropic solid matrix composed mainly of proteoglycans. The preferred fibre alignment is described by a structural tensor entering the strain energy function (Boehler, 1978; Spencer, 1984). Elastin fibers stretch out at low mechanical strains, while the wavy collagen fibers uncrimp without a marked contribution to the overall skin stiffness (Limbert and Taylor, 2002). At higher strains, the stretched cross-linked collagen network carries most of the load up to the characteristic strain locking.

Due to the complex multi-scale hierarchical nature of biological tissues and the resulting difficulties in their experimental characterization, the development of structural models has been limited to favor continuum-based phenomenological hyperelastic and hyper-viscoelastic models (Hurschler et al., 1997; Holzapfel and Ogden, 2009; Criscione et al., 2003; Sacks, 2000). The traditional approach to formulate constitutive laws for biological soft tissues relies on invariant formulations which postulate the existence of a strain energy function depending on a set of tensorial invariants of a certain strain measure. Tensor invariants are selected that characterize the particular deformation modes reproducing real deformations of the tissue. An additive split of the fibre and matrix strain energies is assumed in such phenomenological models that accordingly decouple fibre and matrix effects (Holzapfel et al., 2000; Humphrey, 2003; Humphrey and Yin, 1987; Limbert and Taylor, 2002).

Experimental results reveal the insufficiency of elastic models due to their rough approximation of the actual response, since they ignore the time-dependent behavior of tissues (Prevost et al., 2011; Marchesseau et al., 2010). To address this deficiency, viscoelastic models are used (Fung, 1993; Roylance, 2001). Time-dependent responses of soft biological tissues have been analyzed through monotonic tensile tests at various strain rates and through creep tests (Arumugam et al., 1994; Pioletti et al., 1996; Yanjun et al., 2001; Shergold et al., 2006; Kettaneh et al., 2007). A large number of phenomenological constitutive models have been developed to simulate the experimentally observed anisotropic and time-dependent biomembrane response. The anisotropy is modeled by introducing structural tensors into the constitutive models, as illustrated in, e.g., Humphrey and Yin (1987), Ehret and Itskov (2007), Peña et al. (2011), and Maher et al. (2012). Viscous effects can be modeled using a viscous potential function (Germain, 1973; Pioletti and Rakotomanana, 2000; Roan and Vemaganti, 2011).

Wave propagation in soft biological materials has received considerable attention due to its importance for imaging techniques, which aim at implicit measurements of mechanical properties or visualization of organs (Valdez and Balachandran, 2013). In particular, tissue stiffness measurements can be performed in vivo, through the measurement of shear wave propagation speeds (Sarvazyan et al., 1998; Sandrin et al., 2003; Rouze et al., 2013). The development of accurate models for ultrasound propagation in soft tissues requires the consideration of nonlinear effects in wave propagation, due to the large amplitudes of the acoustic waves. Taking nonlinear effects into account is beneficial for modern ultrasound scanners that employ tissue harmonic imaging, since it provides images with improved clarity and contrast. The attenuation and dispersion of waves, as well as the wave speed, are essential parameters determining the depth reached by the waves and the quality of images. Due to the presence of constituents with viscous properties, soft tissues are absorbing at ultrasonic frequencies with the absorption following a frequency power law. In the context of nonlinear wave propagation, an accurate model of acoustic absorption is of particular importance as the generation of higher frequency harmonics due to nonlinear effects is balanced with their absorption. Furthermore, since soft biological tissues such as biomembranes contain different constituents, including water, their wave propagation characteristics, such as the sound speed and density, are weakly heterogeneous, with variations between the different types of soft tissue of the order of 5% (Krouskop et al., 1987).

The assessment of viscoelastic properties of soft tissues has raised a growing interest in the field of medical imaging in the last two decades, due to the fact that the measurements of local changes of stiffness can be used to detect pathologies. Methods related to dynamic elastography (Krouskop et al., 1987; Lerner et al., 1988; Yamakoshi et al., 1990), such as sonoelastography (Parker and Lerner, 1992; Levinson et al., 1995) or transient elastography (Bercoff et al., 2003; Sandrin et al., 2003), can be used to determine elastic properties of soft biological tissues. Beyond the estimate of second order elastic moduli, the quantification of the nonlinear, anisotropic and viscoelastic effects in soft solids (Catheline et al., 2003, 2004; Bercoff et al., 2004) is an important task that transient elastography is able to address, since the latter images, in real time, the transient propagation of shear waves. Based on the propagation of mechanical shear waves in tissues, diverse elastography techniques have the capability to quantitatively estimate the shear modulus of tissues, in a noninvasive manner (Bercoff et al., 2004; Palmeri et al., 2008; Mitri et al., 2011; Orescanin et al., 2010; Vappou et al., 2009; Hah et al., 2010).

The determination of elasticity model parameters for biological membranes is more involved in comparison to isotropic tissues, due to the occurrence of additional parameters associated with the fibrous microstructure. Initial stresses and/or strains are naturally present in soft biological tissues such as veins, arteries, skin, muscles, ligaments and tendons; for instance, skin is in a state of natural tension. The initial deformation introduces additional effective anisotropy into the wave propagation equations. The anisotropy of the deformation pattern due to either an initial state of finite deformation or to the fibrous microstructure is an important issue for various reasons: the wave speeds in biological materials are directionally dependent, and depend on the level and distribution of the existing deformation, onto which displacements associated with wave propagation are superimposed.

The analysis of nonlinear finite-amplitude wave propagation in biological tissues requires reliable models of fiber-reinforced anisotropic materials, which can take into account hyperelastic and viscoelastic effects. Since the pioneering contribution of (Toupin and Bernstein, 1961), based on the superimposition of small-amplitude oscillations on a finite initial homogeneous deformation, subsequent contributions followed (Thurston, 1965; Biot, 1965; Truesdell and Noll, 2004; Tokuoka and Saito, 1969), showing in particular that pure longitudinal and pure transverse waves can only propagate in the so-called specific directions, depending on material symmetries (Boulanger et al., 1994). The common adopted framework for treating such wave propagation problems is that of incremental waves based on linear approximations of the field equations, leading to incremental equilibrium (Ogden, 2007); fewer works consider the more general and more involved case of finite amplitude waves. The situation with the nonlinear dynamical theory of elasticity contrasts with the flourishing activity in the field of nonlinear elastostatics, especially for incompressible materials, starting from the landmark paper of Rivlin (1947). This is reflected by the fact that few closed-form exact solutions of the full governing dynamical equations have been found (see, e.g., Saccomandi, 2007; Cheviakov and Ganghoffer, 2012; Cheviakov et al., 2015 and references therein). The derivation of exact solutions for BVPs of nonlinear dynamical elasticity is an important and challenging problem nowadays. Even simplistic exact and approximate solutions for symmetry-reduced or simplified elastodynamic configurations are of value for the applications mentioned above, both for providing insights into the physics of the model and for the development and testing of specific numerical methods.

Modern methods of symmetry and conservation law analysis of differential equations (DEs) provide a framework for the systematic study of analytical properties of DE systems and boundary value problems (e.g., Olver, 2000; Bluman and Kumei, 1989; Bluman et al., 2010; Ibragimov, 1994). Similarity and symmetry-invariant solutions of partial differential equations (PDEs) arising in elasticity and plasticity theory have attracted the attention of researchers in recent years (see, e.g., Cheviakov et al., 2015 and references therein). Local conservation laws of DEs contain fundamental, coordinate-invariant information about the structure of the model. For a system of time-dependent partial differential equations $\{R^\sigma(t,\mathbf{x},\mathbf{u},\ldots)\equiv R^\sigma[\mathbf{u}]=0\}_{\sigma=1}^N$ with independent variables t, $\mathbf{x}=\{x^i\}_{i=1}^n$ and dependent variables $\mathbf{u}=\{u^k(t,\mathbf{x})\}_{k=1}^m$, local conservation laws are given by divergence expressions

$$\mathrm{D}_t\Theta+\mathrm{D}_i\Phi^i=0, \tag{1.1}$$

where D_t and $\mathrm{D}_{x^i}\equiv\mathrm{D}_i$ are total derivatives with respect to t and x^i, and the differential functions $\Theta=\Theta[\mathbf{u}]$ and $\Phi^i=\Phi^i[\mathbf{u}]$ are the conservation law density and spatial fluxes respectively. (Summation in repeated indices is assumed where appropriate.)

Knowledge of local conservation laws (1.1) is essential for the analysis of existence, uniqueness and stability of solutions of nonlinear PDEs, as well as for the construction of linearizations and exact and approximate solutions; moreover, modern numerical methods, such as finite element, finite volume, and discontinuous Galerkin methods, require the differential equations in divergence form, or significantly simplify when this is the case (see, e.g., Lax, 1968; Benjamin, 1972; Knops and Stuart, 1984; Anco et al., 2008; Bluman et al., 2008, 2010; LeVeque, 1992 and references therein). The existence of an infinite set of local conservation laws admitted by a PDE model may be indicative of a special structure of model equations, such as integrability or invertible linearization. For reduced models formulated in terms of ordinary differential equations (ODE), local conservation laws yield first integrals, and are used to reduce the order and sometimes completely integrate the differential equations.

If the spatial fluxes Φ^i of a local conservation law vanish on the boundary of the spatial domain $\mathcal{D}$, as well as in the periodic case, the divergence theorem applied to (1.1) yields a global conserved quantity given by

$$\mathcal{J}=\int\int_D\int\Theta\,dV,\quad \frac{d\mathcal{J}}{dt}=0. \tag{1.2}$$

In elasticity theory, a well-known application of conservation laws is the Eshelby energy–momentum tensor, and related path-independent integrals, which govern the energy release rate at a singularity (Budiansky and Rice, 1973; Hatfield and Olver, 1998).

For totally nondegenerate PDE systems, which include the vast majority of physical models, local conservation laws can be represented in terms of linear combinations of the given differential equations (Olver, 2000; Bluman et al., 2010):

$$\mathrm{D}_t\Theta+\mathrm{D}_i\Phi^i=\Lambda_\sigma[\mathbf{u}]R^\sigma[\mathbf{u}]=0, \tag{1.3}$$

for some conservation law multipliers $\{\Lambda_\sigma[\mathbf{u}]\}_{\sigma=1}^N$. The characteristic form (1.3) is the foundation of the systematic *direct conservation law construction method* (Anco and Bluman, 1997; Olver, 2000; Bluman et al., 2010) (for details, see Appendix A). For models arising from a variational principle, Noether's first theorem establishes a correspondence between conservation laws and variational symmetries of the model. In practical computations, however, the direct method is often a preferred way of conservation law computations, for both variational and non-variational models (Bluman et al., 2009), since it requires simpler calculations. In the current contribution, the direct method is employed to compute local conservation laws of several wave propagation models in elastic and viscoelastic fiber-reinforced materials.

The main objective of this paper is the derivation of one-dimensional PDEs and conservation laws describing the propagation of finite-amplitude waves in soft biological tissues modeled within the framework of incompressible nonlinear hyperelasticity and viscoelasticity.

The contribution is organized as follows. In Section 2, hyperelasticity and hyper-viscoelasticity equations and basic constitutive models of elastic materials used in the paper are reviewed. In Section 3, a one-dimensional nonlinear wave equation describing incompressible anti-plane shear displacements for a single fiber family, for the fiber orientation along a constant unit vector of an arbitrary direction, is derived. Equivalence transformations are computed, invertibly relating the general PDE for any fiber direction angle γ to the simpler PDE for $\gamma=0$. Analytical properties of the nonlinear wave equations are studied, including the loss of hyperbolicity condition, wave breaking, and the Lagrangian density for a variational formulation. Local conservation laws and global conserved quantities

are computed. A sample numerical solution exhibiting d'Alembert-type traveling wave splitting is presented.

In Section 4, a system of coupled nonlinear wave equations is presented which describes planar shear waves, i.e., displacements orthogonal to an axis, in the case of a single fiber family. Equivalence transformations are derived, which again invertibly relate the equations for an arbitrary fiber orientation angle with simpler ones corresponding to zero fiber angle. Local conservation laws are systematically computed. A variational formulation (a physical Lagrangian) is derived. Symmetry properties and exact solutions of the PDE system describing the planar shear waves with fibers along the propagation direction (fiber angle $\gamma = 0$) have been previously considered in Cheviakov et al. (2015). Through the newly derived invertible equivalence transformations, the results of Cheviakov et al. (2015) are generalized onto the case of arbitrary fiber orientation.

In Section 5, anti-plane shear waves in a general two-fiber model are studied. The model provides a "flat cylinder" approximation of an arterial wall setup (Holzapfel et al., 2000). An explicit expression for the hydrostatic pressure and a hyperbolic nonlinear PDE satisfied by the displacement are derived. It is shown that the PDE can be invertibly mapped into a simple generic nonlinear wave equation of Section 3. A numerical computation illustrating sample fiber displacements is presented.

Section 6 provides a generalization of Section 3 results to include viscoelastic effects. It is shown that one-dimensional anti-plane shear type displacements satisfy a nonlinear PDE involving third-order mixed space–time derivatives in the damping term. Basic local conservation laws are computed, and a potential system is constructed. Unlike the initial PDE, the potential system has a simpler form of coupled evolution equations. The potential system is used for a numerical computation, in which the wave shape evolution is compared to that in the inviscid case.

Symbolic conservation law computations in the current paper were performed using the `GeM` software package for `Maple` (Cheviakov, 2007, 2010a, 2014). Numerical results were obtained using `Matlab` and `COMSOL` software.

2. Incompressible dynamic models of fiber-reinforced materials

The continuum governing equations and a number of constitutive models relevant to the description of anisotropic hyperelastic and hyper-viscoelastic materials exhibiting incompressible behavior are now considered. In Sections 3–6, these models are applied to the study of nonlinear wave propagation in specific symmetric configurations.

2.1. *Hyperelastic models*

Suppose an elastic body occupies a material (Lagrange) spatial region $\overline{\Omega}_0 \subset \mathbb{R}^3$, where Ω_0 is an open bounded connected set having a Lipschitz boundary (Ciarlet, 1988; Marsden and Hughes, 1994). The corresponding domain in the actual (Eulerian) frame is denoted by $\overline{\Omega} = \phi(\overline{\Omega}_0) \subset \mathbb{R}^3$. The position $\mathbf{x} = (x^1, x^2, x^3) \in \overline{\Omega}$ of a material point depends on the Lagrange coordinates $\mathbf{X} = (X^1, X^2, X^3) \in \overline{\Omega}_0$ at time t according to

$$\mathbf{x} = \phi(\mathbf{X}, t),$$

where the mapping ϕ is sufficiently smooth. The deformation gradient is given by

$$\mathbf{F}(\mathbf{X}, t) = \nabla\phi, \quad F^i_j = \frac{\partial \phi^i}{\partial X^j} = F_{ij}. \tag{2.1}$$

In this work, we study models described by incompressible motions, which satisfy the incompressibility condition

$$J = \det \mathbf{F} = 1.$$

For incompressible materials, the reference and actual mass densities are equal:

$$\rho(\mathbf{X}, t) = \rho_0(\mathbf{X})/J = \rho_0(\mathbf{X}),$$

and are assumed time-independent.

The stress in the reference configuration is described by the first Piola–Kirchhoff tensor $\mathbf{P}$, or a related second Piola–Kirchhoff tensor $\mathbf{S} = \mathbf{F}^{-1}\mathbf{P}$. For *anisotropic hyperelastic* materials, a scalar volumetric strain energy density function $W^h = W^h(\mathbf{X}, \mathbf{F}, \mathbf{A}_1, \ldots, \mathbf{A}_k)$ in the reference configuration is prescribed, defining the material behavior. Here the unit column vectors $\mathbf{A}_j, j = 1, \ldots, k$, define k independent fiber families. An isotropic hyperelastic model corresponds to $k = 0$. For anisotropic models, it is common to use the form of the strain energy density

$$W^h = W_{iso} + W_{aniso} \tag{2.2}$$

a sum of an isotropic and an anisotropic contribution (e.g., Basciano and Kleinstreuer, 2009).

For incompressible models, the first and the second Piola–Kirchhoff tensors are respectively given by the formulas

$$\mathbf{P} = -p\,\mathbf{F}^{-T} + \frac{\partial W^h}{\partial \mathbf{F}} = \mathbf{F}\,\mathbf{S}, \tag{2.3}$$

$$\mathbf{S} = -p\,\mathbf{C}^{-1} + 2\frac{\partial W^h}{\partial \mathbf{C}}, \tag{2.4}$$

where $p = p(\mathbf{X}, t)$ is the hydrostatic pressure, and $\mathbf{C} = \mathbf{F}^T\mathbf{F}$ is the right Cauchy–Green deformation tensor. Since $\mathbf{C}$ is symmetric, the formula (2.4) is understood in the sense

$$\frac{\partial W^h}{\partial \mathbf{C}} \equiv \frac{1}{2}\left(\frac{\partial W^h}{\partial \mathbf{C}} + \frac{\partial W^h}{\partial \mathbf{C}^T}\right).$$

A constitutive relation for an incompressible isotropic homogeneous hyperelastic material is usually given as an expression of the strain energy density $W^h = W^h(I_1, I_2)$ in terms of the principal invariants of $\mathbf{C}$:

$$I_1 = \mathrm{Tr}\,\mathbf{C}, \quad I_2 = \tfrac{1}{2}\left[(\mathrm{Tr}\,\mathbf{C})^2 - \mathrm{Tr}(\mathbf{C}^2)\right]. \tag{2.5}$$

(For compressible materials, $W^h = W^h(I_1, I_2, I_3)$ with $I_3 = \det \mathbf{C} = J^2$.) A wide class of materials, including rubber-like hyperelastic materials, is described by the *Mooney–Rivlin* constitutive relation:

$$W_{iso} = a(I_1 - 3) + b(I_2 - 3) \tag{2.6}$$

with material parameters $a, b > 0$ (measured in the units of pressure); the case $b = 0$ is referred to as the *Neo-Hookean* model.

For anisotropic hyperelastic materials, the energy contribution W_{aniso} in (2.2) is commonly assumed to depend on pseudo-invariants involving fiber direction vectors $\{\mathbf{A}_j\}_{j=1}^k$. For a single fiber family, for example, one has $W_{aniso} = W_{aniso}(I_4, I_5)$, with

$$I_4 = \mathbf{A}_1^T\mathbf{C}\mathbf{A}_1, \quad I_5 = \mathbf{A}_1^T\mathbf{C}^2\mathbf{A}_1. \tag{2.7}$$

For two fiber families, one can have, generally,

$$W_{aniso} = W_{aniso}(I_4, I_5, I_6, I_7, I_8, I_9), \tag{2.8}$$

depending on four pseudo-invariants

$$I_4 = \mathbf{A}_1^T \mathbf{C} \mathbf{A}_1, \quad I_5 = \mathbf{A}_1^T \mathbf{C}^2 \mathbf{A}_1, \quad I_6 = \mathbf{A}_2^T \mathbf{C} \mathbf{A}_2, \quad I_7 = \mathbf{A}_2^T \mathbf{C}^2 \mathbf{A}_2, \tag{2.9}$$

and possibly on the interaction pseudo-invariants (e.g., Holzapfel, 2000)

$$I_8 = (\mathbf{A}_1^T \mathbf{A}_2) \mathbf{A}_1^T \mathbf{C} \mathbf{A}_2, \quad I_9 = (\mathbf{A}_1^T \mathbf{A}_2)^2. \tag{2.10}$$

The quantities I_4, I_6 measure the squared stretch factor λ given by

$$\lambda \mathbf{a}_j = \mathbf{F} \mathbf{A}_j \tag{2.11}$$

along the fiber directions $\mathbf{A}_j, j = 1, 2$. The pseudo-invariants I_5, I_7 are related to the effect of the fiber on the shear response in the material (Demirkoparan et al., 2010; Merodio and Ogden, 2005; Pandolfi and Manganiello, 2006). The pseudo-invariant I_8 provides coupling between the two sets of fibers; it is used in specific models such as that of the cornea (Pandolfi and Manganiello, 2006). The quantity I_9 is an inner product of fiber direction vectors in the material configuration.

The full system of equations of motion of an incompressible hyperelastic material in three dimensions is given by the balance of momentum vector equation and the scalar incompressibility condition:

$$\rho_0 \mathbf{x}_{tt} = \mathrm{div}_{(\mathbf{x})} \mathbf{P} + \rho_0 \mathbf{R}, \quad J = \det \mathbf{F} = 1. \tag{2.12}$$

In (2.12), $\mathbf{R} = \mathbf{R}(\mathbf{X}, t)$ is the total body force per unit mass.

Remark 2.1. It is important to note that when the body forces are absent or potential, the nonlinear PDE model (2.12) follows from a classical variational principle. In particular, when $\mathbf{R} = 0$, the Lagrangian density is given by

$$\mathcal{L} = -K + W^h - p(J-1), \tag{2.13}$$

where $K = \frac{1}{2}\rho_0(\dot{\mathbf{x}})^2$ is the kinetic energy density. (Here and below, where appropriate, the dot denotes the time derivative.) The four equations (2.12) arise as the Euler–Lagrange equations through the action of Euler differential operators with respect to components of $\mathbf{x}$ and the pressure p on the Lagrangian density (2.13) (see, e.g., Holzapfel, 2000; Cheviakov and St. Jean, 2015).

2.2. *Hyper-viscoelastic models*

A significant number of practically important materials exhibit, over specific ranges of stress and time, essentially viscoelastic behavior. Due to the complexity of the microstructural evolutions occurring within a material body, the constitutive modelling of the response of inelastic materials has no unique formulation. Thermodynamics offers a convenient framework for the development of constitutive equations (see, e.g., Hutter, 1977 for a review of various approaches). One can distinguish two different theories, 'rational thermodynamics' and 'irreversible thermodynamics' (see De Groot, 1951; Bataille and Kestin, 1979 for the works of their proponents). Irreversible thermodynamics differs from rational thermodynamics in the use of internal variables to account for history effects (dissipation) of the material. Approaches based on non-equilibrium thermodynamics prove useful as a framework for the derivation of generic constitutive laws, as well as specific constitutive models. The most widely spread existing theory relies on the notion of a local state, and involves a single potential, which includes the state laws (reversible part of the constitutive laws) and a dissipation (or pseudo-dissipation) potential for the description of its irreversible part (see Biot, 1954). Thereby, Biot laid down a variational formulation for nonlinear viscous phenomena including dynamics, based on d'Alembert's principle. Such approach has proven adequate for the description of a wide range of materials and a broad spectrum of dissipative behavior types, including standard, standard generalized, rate dependent (viscoplasticity), and rate independent (plasticity) ones. Alternative theories, such as rational thermodynamics and its generalizations (e.g., Coleman and Noll, 1963; Truesdell and Noll, 2004; Caruthers et al., 2004), go beyond the local equilibrium assumption. Finite viscoelasticity models, which can account for large deformation rates by considering large deviations away from thermodynamic equilibrium, have been developed in, for example, Reese and Govindjee (1998), Sidoroff (1974), Haupt (1993a,b), Lubliner (1985), Le Tallec et al. (1993), and Dafalias (1991). Linear viscoelasticity theory restricts to small deviations from thermodynamic equilibrium (see, e.g., Coleman and Noll, 1961). Various other models have been suggested, including phenomenological ones (Ogden and Holzapfel, 2006) and quasi-linear viscoelasticity models (Fung, 1993; Abramowitch and Woo, 2004; Toms et al., 2002). For a review, see, for example, Boubaker (2009).

In the present work, we adopt the hyper-viscoelasticity approach of Holzapfel (2000), based on the use of a hyperelastic potential to describe purely elastic effects, and a viscous "dissipative potential" associated to purely viscous phenomena. The total stress consequently is given by the sum of an elastic and a viscous stress. (A similar additive decomposition would be obtained using Biot's approach.)

In Holzapfel (2000) and related works, the hyperelastic strain energy density function $W = W^h$ is modified to additively include the viscous potential:

$$W = W^h + W^v. \tag{2.14}$$

The dissipative potential W^v may incorporate terms describing short-term elasticity effects through pseudo-invariants that depend on $\dot{\mathbf{C}}$, as well as integral terms describing the long-term viscoelastic response. For example, in Pioletti and Rakotomanana (2000), in order to account only for short-term elastic effects, an expression

$$W^v = \frac{\eta}{4} J_2 (I_1 - 3), \quad J_2 = \mathrm{Tr}\left(\dot{\mathbf{C}}^2\right) \tag{2.15}$$

is employed. Similarly, in Merodio and Goicolea (2007), within a viscoelastic model of a fiber-reinforced material, the dissipative potential is suggested in the form

$$W^v = \frac{\eta_1}{4} J_2 (I_1 - 3) + \eta_2 J_9 \frac{k_1}{2k_2} \left(e^{k_2 (I_4 - 1)^2} - 1 \right), \quad \eta_1, \eta_2 = \mathrm{const}, \tag{2.16}$$

involving both the pseudo-invariant J_2 and an additional fiber-dependent pseudo-invariant:

$$J_9 = \mathbf{A}^T (\dot{\mathbf{C}}^2) \mathbf{A}. \tag{2.17}$$

The two terms of W^v (2.16) replicate the two terms of the hyperelastic strain energy density W^h used in that work.

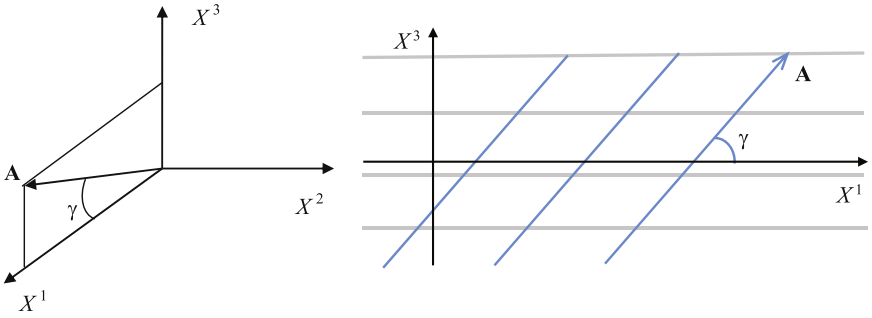

Fig. 1 – One-dimensional hyperelastic anti-plane shear motions: fiber orientation.

Using the combined hyperelastic-dissipative potential (2.14), one consequently computes the modified second Piola–Kirchhoff tensor:

$$\mathbf{S} = \mathbf{S}^h + \mathbf{S}^v = \left[-p\,\mathbf{C}^{-1} + 2\,\frac{\partial W^h}{\partial \mathbf{C}}\right] + \left[2\frac{\partial W^v}{\partial \dot{\mathbf{C}}}\right]. \tag{2.18}$$

For (2.15), for example, one has

$$\mathbf{S}^v = \eta(I_1 - 3)\dot{\mathbf{C}}.$$

3. One-dimensional hyperelastic anti-plane shear motions

As a first specific model, we consider an incompressible hyperelastic material reinforced with a single family of fibers. This situation is representative of elongated soft biological tissues like muscles. Let the strain energy density be given by

$$W^h = a(I_1 - 3) + b(I_2 - 3) + q(I_4 - 1)^2, \tag{3.1}$$

with anisotropy material parameter $q = \text{const} > 0$, i.e., a combination of the Mooney–Rivlin and the standard (quadratic) reinforcement terms. We note that the anisotropic term in (3.1) corresponds to the first term of the Taylor series expansion of a general analytic even function of $I_4 - 1$, for example, the exponential model of Merodio and Goicolea (2007).

Consider the following motions explicitly compatible with the incompressibility condition:

$$\mathbf{x} = \begin{bmatrix} X^1 \\ X^2 \\ X^3 + G(X^1, t) \end{bmatrix}. \tag{3.2}$$

The ansatz (3.2) describes the propagation of the displacements in the direction of X^3 along the axis of X^1, i.e., the anti-plane shear motions. With no additional assumptions made on the finite displacement $G(X^1, t)$, one indeed has $J \equiv 1$.

Let the fiber family be directed along a generic unit material vector

$$\mathbf{A} = \begin{bmatrix} \cos\gamma \\ 0 \\ \sin\gamma \end{bmatrix} \tag{3.3}$$

in the (X^1, X^3) plane (Fig. 1).

The substitution of (3.1)–(3.3) into the momentum equations in (2.12) with zero body forces yields a single scalar nonlinear wave equation on the displacement $G(X^1, t)$, and the hydrostatic pressure is computed explicitly. Using a simplified notation

$$X^1 = x, \quad G = G(x,t), \quad p = p(x,t), \quad \alpha = 2(a + b)/\rho_0 > 0, \quad \beta = 4q/\rho_0 > 0, \tag{3.4}$$

one finds that the pressure is given by

$$p = \beta\rho_0 \cos^3\gamma(\cos\gamma G_x + 2\sin\gamma)G_x + f(t), \tag{3.5}$$

where $f(t)$ is an arbitrary gauge determined by the boundary conditions. The transverse displacement $G(x,t)$ satisfies a nonlinear wave equation

$$G_{tt} = \left(\alpha + \beta\cos^2\gamma\left(3\cos^2\gamma(G_x)^2 + 6\sin\gamma\cos\gamma G_x + 2\sin^2\gamma\right)\right)G_{xx}. \tag{3.6}$$

Two important special cases arise.

Case 1: $\gamma = \pi/2$. When the fibers are directed along X^3, the displacement $G(x,t)$ is independent of the fiber direction; the fiber-dependent terms in the dynamic equation vanish, and the nonlinear equation (3.6) reduces to a linear wave equation

$$G_{tt} = \alpha G_{xx}, \quad p_x = 0. \tag{3.7}$$

Case 2: $\gamma = 0$. When the fibers are directed along the wave propagation direction $x = X^1$, the PDE (3.6) reduces to a nonlinear wave equation

$$G_{tt} = (3\beta G_x^2 + \alpha)G_{xx}, \tag{3.8}$$

and the pressure (3.5) simplifies to

$$p = \beta\rho_0 G_x^2 + f(t). \tag{3.9}$$

Since $\alpha, \beta > 0$, the PDE (3.8) is strictly hyperbolic; indeed, a one-to-one point transformation

$$x = L\hat{x}, \quad t = L\alpha^{-1/2}\hat{t}, \quad G(x,t) = L\left(\frac{\alpha}{3\beta}\right)^{1/2}\hat{G}(\hat{x},\hat{t}) \tag{3.10}$$

maps Eq. (3.8) into a dimensionless PDE

$$\hat{G}_{\hat{t}\hat{t}} = (\hat{G}_{\hat{x}}^2 + 1)\hat{G}_{\hat{x}\hat{x}} \tag{3.11}$$

containing no parameters. In (3.10), $L > 0$ (m) is an arbitrary characteristic length scale.

3.1. *Equivalence transformations and the independence on the fiber angle γ*

For a PDE model that contains $M \geq 1$ constitutive functions and/or parameters $K=(K_1, \ldots, K_M)$, *equivalence transformations* are transformations that map existing independent variables $\{x^i\}$, dependent variables $\{u^i\}$, and the constitutive functions/parameters into other variables and functions/parameters, so that the form of the PDEs is preserved. Knowledge of the equivalence transformations lets one efficiently reduce the number of significant parameters, and simplify the classes of constitutive functions the model involves (see, e.g., Ovsiannikov, 1982; Bluman et al., 2010). Most common equivalence transformations include, for example, scalings and translations. The scaling transformation (3.10) for the PDE family (3.8) involving two constitutive parameters is an example of an equivalence transformation.

The nonlinear wave equation (3.6) involves three constitutive parameters: two material parameters α, β and the fiber angle γ. Consequently, a Lie group of equivalence transformations can be represented by an infinitesimal generator

$$X = \xi^1 \frac{\partial}{\partial x} + \xi^2 \frac{\partial}{\partial t} + \eta \frac{\partial}{\partial G} + \zeta^1 \frac{\partial}{\partial \alpha} + \zeta^2 \frac{\partial}{\partial \beta} + \zeta^3 \frac{\partial}{\partial \gamma}. \tag{3.12}$$

A direct computation following the Lie's algorithm yields three equivalence transformations; they have the simplest forms in terms of $\tan\gamma$ rather than γ itself, and are given by the generators

$$\begin{aligned} X_1 &= -\frac{t}{2}\frac{\partial}{\partial t} + \alpha\frac{\partial}{\partial \alpha} + \beta\frac{\partial}{\partial \beta}, \\ X_2 &= -x\frac{\partial}{\partial G} + 2\beta \sin\gamma \cos^3\gamma \frac{\partial}{\partial \alpha} + 4\beta \sin\gamma \cos\gamma \frac{\partial}{\partial \beta} + \frac{\partial}{\partial(\tan\gamma)}, \\ X_3 &= -x\frac{\partial}{\partial x} + 2\alpha\frac{\partial}{\partial \alpha} + 4\beta \cos^2\gamma \frac{\partial}{\partial \beta} + (\tan\gamma)\frac{\partial}{\partial(\tan\gamma)}. \end{aligned} \tag{3.13}$$

The transformation generator X_1 corresponds to the scaling of t, α, β. The finite transformation corresponding to the generator X_1 is given by

$$\tilde{\alpha} = S\alpha, \quad \tilde{\beta} = S\beta, \quad \tilde{t} = S^{-1/2}t, \quad S \in \mathbb{R},$$

and can be used to set, for example, $\tilde{\alpha}$ or $\tilde{\beta}$ to equal 1.

The generator X_2 in (3.13) yields shifts in $\tan\gamma$, having the global group form

$$\begin{aligned} &\tilde{G} = G - sx, \quad \tan\tilde{\gamma} = \tan\gamma + s, \\ &\tilde{\alpha} = \alpha + 2\beta\cos^4\gamma\left(\frac{s^2}{2} + s\tan\gamma\right), \quad \tilde{\beta} = \beta\cos^4\gamma(\tan^2\gamma \\ &\quad + 2s\tan\gamma + s^2 + 1)^2, \end{aligned}$$

with a group parameter $s \in \mathbb{R}$. In particular, the choice of $s = -\tan\gamma$ lets one map the PDE (3.6) into one with $\tan\tilde{\gamma} = \tilde{\gamma} = 0$, i.e., into the simpler PDE (3.8) written in terms of the corresponding quantities with tildes. The transformation is given by

$$\begin{aligned} &x = \tilde{x}, \quad t = \tilde{t}, \quad G = \tilde{G} - x\tan\gamma, \quad \alpha = \tilde{\alpha} \\ &\quad + \tilde{\beta}\tan^2\gamma, \quad \beta = \tilde{\beta}\cos^{-4}\gamma, \end{aligned} \tag{3.14}$$

Substituting (3.14) into the full PDE (3.6) yields

$$\tilde{G}_{tt} = (3\tilde{\beta}\tilde{G}_x^2 + \tilde{\alpha})\tilde{G}_{xx} \tag{3.15}$$

with

$$\tilde{\alpha} = \alpha - \frac{\beta}{4}\sin^2 2\gamma, \quad \tilde{\beta} = \beta\cos^4\gamma.$$

which is Eq. (3.8) up to the omission of the tildes. Unlike the PDE (3.8), Eq. (3.15) involves the parameter $\tilde{\alpha}$ that is not necessarily positive.

Remark 3.1. Equivalence transformations corresponding to the generators X_2 and X_3 become degenerate in the special case $\gamma = \pi/2$, when the PDE (3.6) is equivalent to Eq. (3.7) instead of (3.8).

Remark 3.2. The *loss of hyperbolicity* of the PDE model (3.6), or equivalently (3.15), can occur when the coefficient of G_{xx} (respectively, $\tilde{G}_{xx}$) vanishes or changes sign. This may happen for certain solutions when the coefficient of G_{xx}, a quadratic expression in terms of G_x (respectively, $\tilde{G}_x$), has a nonnegative discriminant. The latter is the case when $\tilde{\alpha} \leq 0$. Hence the necessary (but not sufficient) condition for the loss of hyperbolicity in the PDE (3.6) is given by

$$\sin^2(2\gamma) \geq \frac{4\alpha}{\beta}. \tag{3.16}$$

Clearly, (3.16) can only hold for special fiber orientations γ if the fiber strength provided by the material parameter β is significantly large (cf. Cheviakov et al., 2015). In the further analysis, the boundary case

$$\sin^2(2\gamma) = \frac{4\alpha}{\beta} \tag{3.17}$$

plays an important role.

Remark 3.3. Since in the transformation of (3.6)–(3.15), $\tilde{\beta} > 0$, but $\tilde{\alpha}$ may be positive, negative or zero, it is clear that a further transformation similar to (3.10) can map the PDE (3.6) into

$$\hat{G}_{\hat{t}\hat{t}} = (\hat{G}_{\hat{x}}^2 + K)\hat{G}_{\hat{x}\hat{x}}, \quad \hat{G} = \hat{G}(\hat{x}, \hat{t}), \quad K = \mathrm{Sign}\,\tilde{\alpha} = \begin{cases} 1, & \tilde{\alpha} > 0; \\ -1, & \tilde{\alpha} < 0; \\ 0, & \tilde{\alpha} = 0 \end{cases} \tag{3.18}$$

(cf. (3.11)). For this PDE family, it is clear that the loss of hyperbolicity may occur only when $K=0$ or $K=-1$.

3.2. *Analytical properties of the nonlinear wave equations (3.18)*

In Section 3.1, it has been shown that the one-dimensional anti-plane shear equation (3.6) for any fiber orientation γ is in a one-to-one local correspondence with a PDE of the class (3.18). This class of equations has been well-studied in the literature. We now discuss some of its basic properties. Within this section, for the simplicity of notation, all hats in the dimensionless variables are omitted.

(a) *A variational formulation*: Any PDE of the class (3.18) follows from a variational principle, with the Lagrangian density given (up to equivalence) by the formula

$$\mathcal{L} = \tfrac{1}{12}G_x^4 + \tfrac{1}{2}KG_x^2 - \tfrac{1}{2}G_t^2. \tag{3.19}$$

Due to the existence of the variational formulation, according to Noether's theorem, there is a one-to-one correspondence between equivalence classes of variational symmetries and local conservation laws (e.g., Olver, 2000).

(b) *Local conservation laws*: Local conservation laws for the current model can be systematically sought using the

direct method (Appendix A). The following conservation laws hold for the PDE family (3.18), and consequently, for the equivalent full one-fiber physical model (3.6), for an arbitrary fiber family orientation.

1. The local conservation of the Eulerian momentum in the perturbation direction X^3 follows from the multiplier $\Lambda = 1$, and corresponds to the Eulerian spatial translation symmetry $\partial/\partial G$:

$$D_t(G_t) - D_x\left(G_x\left(\tfrac{1}{3}G_x^2 + K\right)\right) = 0. \tag{3.20}$$

For example, for finite perturbations with a compact support, $S \subset \mathbb{R}$, the conserved linear momentum is a constant of motion given by

$$M_{(X^3)} = \int_S G_t(x,t)\,dx, \quad \frac{d}{dt}M_{(X^3)} = 0. \tag{3.21}$$

Global conserved quantities for other local conservation laws below are computed in a similar manner.

2. The conservation of Lagrangian momentum corresponds to the multiplier $\Lambda = G_x$ and the Lagrangian spatial translation symmetry $\partial/\partial x$. It is given by the divergence expression

$$D_t(G_xG_t) - D_x\left(\tfrac{1}{2}\left(G_t^2 + KG_x^2\right) + \tfrac{1}{4}G_x^4\right) = 0. \tag{3.22}$$

3. The local conservation of energy

$$D_t\left(\tfrac{1}{2}\left(G_t^2 + KG_x^2\right) + \tfrac{1}{12}G_x^4\right) - D_x\left(G_tG_x\left(\tfrac{1}{3}G_x^2 + K\right)\right) = 0 \tag{3.23}$$

arises from the multiplier $\Lambda = G_t$. The corresponding symmetry is the time-translation $\partial/\partial t$. The total energy, if it is finite, is a constant of motion given by

$$E = \int_S \left(\tfrac{1}{2}\left(G_t^2 + KG_x^2\right) + \tfrac{1}{12}G_x^4\right)dx = \text{const}.$$

4. A conservation law following from the multiplier $\Lambda = t$ has the form

$$D_t(G - tG_t) + D_x\left(tG_x\left(\tfrac{1}{3}G_x^2 + K\right)\right) = 0. \tag{3.24}$$

It is well-known in mechanics (see, e.g., Olver, 2000, p. 279), and may be called the "center of mass theorem" in models where G represents mass density. The corresponding variational symmetry is the Galilei transformation $t\partial/\partial G$. The related global conserved quantity, in conjunction with (3.21), yields

$$\int_S G(x,t)\,dx - tM_{(X^3)} = C = \text{const},$$

describing the rate of change of the average displacement.

5. An infinite number of conservation laws of (3.18) can be shown to arise from local multipliers $\Lambda(G_t, G_x)$ given by solutions of a linear PDE:

$$\Lambda_{G_x,G_x} = \left(G_x^2 + K\right)\Lambda_{G_t,G_t}. \tag{3.25}$$

Due to the self-adjoint nature of the PDE family (3.18), these multipliers are equivalent to a set of contact variational symmetries $\hat{X} = \theta(G_t, G_x)\partial/\partial G$ (3.18) (see also Bihlo et al., 2012). Such an infinite set of local conservation laws or contact symmetries can be used to construct a Legendre contact transformation (Anco et al., 2008; Kumei and Bluman, 1982; Bluman et al., 2010):

$$u = G_x, \quad v = G_t, \quad W(u,v) = G(x,t) - xG_x - tG_t,$$

which invertibly maps each nonlinear PDE (3.18) into a linear wave equation

$$W_{uu} = (u^2 + K)W_{vv}. \tag{3.26}$$

6. Higher-order conservation laws of the PDEs (3.18) exist. An example of a conservation law corresponding to a third-order multiplier is given by

$$D_t\frac{G_{xx}}{G_{tx}^2 - (G_x^2 + K)G_{xx}^2} + D_x\frac{G_{tx}}{G_{tx}^2 - (G_x^2 + K)G_{xx}^2} = 0. \tag{3.27}$$

The physical interpretation of the conserved density in (3.27) remains to be studied. The family of PDEs (3.18) can have further higher-order conservation laws, which may be, however, harder to compute.

7. When $K=0$, Eq. (3.18) reads $G_{tt} = G_x^2G_{xx}$. It can be shown to have an additional variational symmetry $\hat{Y} = (G - 3xG_x - 5tG_t)\partial/\partial G$ (see Cheviakov et al., 2015), which is a scaling symmetry. According to Noether's theorem, one has the corresponding conservation law multiplier $\Lambda = G - 3xG_x - 5tG_t$. The local conservation law is given by

$$\begin{aligned} &D_t\left(GG_t - \tfrac{5}{2}t\left[G_t^2 + \tfrac{1}{6}G_x^4\right] - 3xG_tG_x\right) \\ &\quad - D_x\left(\tfrac{1}{3}GG_x^3 - \tfrac{5}{3}tG_tG_x^3 - \tfrac{3}{2}x\left[G_t^2 + \tfrac{1}{2}G_x^4\right]\right) = 0. \end{aligned} \tag{3.28}$$

The analogs of the conservation law (3.28) hold for the general nonlinear wave equation (3.6) with an arbitrary fiber direction when the condition (3.17) is satisfied.

(c) *Wave breaking*: The squared characteristic speed $c^2 = G_x^2 + K$ of (3.18) is variable, hence points on the solution curve corresponding to higher values of the curve slope $|G_x|$ will yield higher characteristic speeds. Depending on the initial data, this may lead to the intersection of characteristic curves and shock formation. Such effects restrict applicability limits of non-dissipative hyperelastic models (cf. Cheviakov et al., 2015; Saccomandi and Vitolo, 2014).

3.3. A sample numerical simulation

For an illustration of solution behavior, we numerically solve the nonlinear wave equation (3.18) with $K=1$ for a stationary Gaussian initial displacement:

$$\hat{G}(\hat{x},0) = \exp(-\hat{x}^2), \quad \hat{G}_{\hat{t}}(\hat{x},0) = 0, \tag{3.29}$$

to obtain a nonlinear D'Alembert-like pair of left- and right-traveling waves (Fig. 2).

The above solution can be used to plot, for example, the material lines $X^1 = \text{const}$ and the fiber lines $X^3 = \text{const}$ for the one-dimensional hyperelastic anti-plane shear PDE (3.8) for the fiber angle $\gamma = 0$. We employ the parameter values

$$\rho_0 = 1.1 \cdot 10^3\ \text{kg/m}^3, \quad a = 1.5 \cdot 10^3\ \text{Pa}, \quad b = 0, \quad q = 1.18 \cdot 10^3\ \text{Pa}, \tag{3.30}$$

which are typical for a rabbit carotid artery media (Holzapfel et al., 2000), in the transformations (3.10). The above numerical solution of the dimensionless PDE (3.18) with the initial Gaussian profile at $\hat{t} = 3$ yields the displacements of the material and fiber lines shown in Fig. 3.

4. Planar shear waves – displacements transverse to an axis

Another class of displacements of interest is given by displacements orthogonal to the X^1 direction:

$$\mathbf{x} = \begin{bmatrix} X^1 \\ X^2 + H(X^1, t) \\ X^3 + G(X^1, t) \end{bmatrix}, \tag{4.1}$$

which again propagate along the direction of X^1, with the single fiber family given by unit vector (3.3) (see Fig. 1). For the motions (4.1), the incompressibility condition is identically satisfied. For this essentially one-dimensional problem, we again employ the simplified notation (3.4), $H = H(x, t)$.

Using the strain energy density (3.1) and the ansatz (4.1) in the equations of motion (2.12) with zero body forces, we find that the pressure equation decouples again, and the hydrostatic pressure can be computed explicitly:

$$p = \beta\rho_0 \cos^3\gamma\left[\cos\gamma(G_x^2 + H_x^2) + 2\sin\gamma\, G_x\right] + f(t)\Big), \tag{4.2}$$

where $f(t)$ is an arbitrary function. As noted in Cheviakov et al. (2015), the PDEs for the displacements $H(x, t)$, $G(x, t)$ have the form

$$\begin{aligned} H_{tt} &= \left(\alpha + \beta\cos^3\gamma\left[2\sin\gamma\, G_x + \cos\gamma\,(3H_x^2 + G_x^2)\right]\right)H_{xx} \\ &\quad + 2\beta\cos^3\gamma\,(\sin\gamma + \cos\gamma\, G_x)H_xG_{xx}, \\ G_{tt} &= 2\beta\cos^3\gamma\,(\sin\gamma + \cos\gamma\, G_x)H_xH_{xx} \\ &\quad + \Big(\alpha + \beta\cos^2\gamma\Big[\cos^2\gamma\,(H_x^2 + 3G_x^2) + 3\sin(2\gamma)\, G_x + 2\sin^2\gamma\Big]\Big)G_{xx}. \end{aligned} \tag{4.3}$$

The PDEs (4.3) are variational. The Lagrangian density in the present case is given by

$$\mathcal{L} = \mathcal{P} - \mathcal{K}, \tag{4.4}$$

where the potential energy is obtained from (3.1) and has the form

$$\begin{aligned} \mathcal{P} = W^h &= \frac{\alpha}{2}(H_x^2 + G_x^2) \\ &\quad + \frac{\beta}{4}\cos^2\gamma\Big[G_x^2(\cos^2\gamma G_x^2 + 2\sin(2\gamma)G_x + 4\sin^2\gamma) \\ &\quad + \cos\gamma H_x^2(\cos\gamma(2G_x^2 + H_x^2) + 4\sin\gamma G_x)\Big]; \end{aligned} \tag{4.5}$$

the kinetic energy is given by

$$\mathcal{K} = \tfrac{1}{2}(H_t^2 + G_t^2). \tag{4.6}$$

The Lagrangian density (4.4) does not involve the pressure term of (2.13), since for the displacements (4.1), $J \equiv 1$.

Special cases arise for the system (4.3) for the fiber angle values $\gamma = \pi/2$ and $\gamma = 0$. For $\gamma = \pi/2$, the fibers are directed along X^3, and both displacements $H(x, t)$ and $G(x, t)$ are independent of the fiber direction. In agreement with Theorem 1 of Cheviakov et al. (2015), such motions are described by independent linear PDEs:

$$H_{tt} = \alpha H_{xx}, \quad G_{tt} = \alpha G_{xx}. \tag{4.7}$$

The second special case corresponding to the fiber angle $\gamma = 0$ yields a symmetric form of the wave equation (4.3):

$$\begin{aligned} H_{tt} &= \alpha H_{xx} + \beta\left(\left[3H_x^2 + G_x^2\right]H_{xx} + 2G_xH_xG_{xx}\right), \\ G_{tt} &= \alpha G_{xx} + \beta\left(2G_xH_xH_{xx} + \left(H_x^2 + 3G_x^2\right)G_{xx}\right). \end{aligned} \tag{4.8}$$

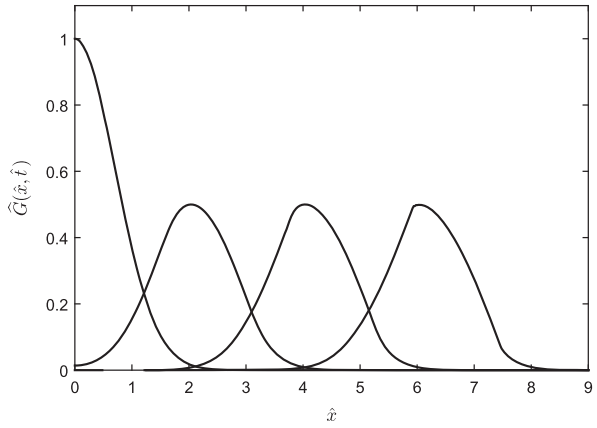

Fig. 2 – Right-traveling wave profiles for the dimensionless PDE (3.18) with $K = 1$ and initial conditions (3.29), for the times $\hat{t} = 0, 2, 4, 6$ (left to right).

Remark 4.1. Similar to the case of the anti-plane shear, equivalence transformations in the form of Lie point transformations can be computed for the general PDE system (4.3). It can be shown that there exists an equivalence transformation that invertibly maps the general PDE system (4.3), for an *arbitrary* fiber direction $\gamma \neq \pi/2$ into the symmetric case (4.8) corresponding to $\gamma = 0$; the two systems are thus mathematically equivalent. This point transformation is given by

$$\begin{aligned} &x = \tilde{x}, \quad t = \tilde{t}, \quad G = \tilde{G} - x\tan\gamma, \quad \alpha = \tilde{\alpha} \\ &\quad + \tilde{\beta}\tan^2\gamma, \quad \beta = \tilde{\beta}\cos^{-4}\gamma. \end{aligned} \tag{4.9}$$

Substitution of (4.9) into (4.3) and the omission of tildes yields the system (4.8) corresponding to the fiber angle $\gamma = 0$.

The parameter transformation obtained by the inversion of (4.9):

$$\tilde{\alpha} = \alpha - \frac{\beta}{4}\sin^2 2\gamma, \quad \tilde{\beta} = \beta\cos^4\gamma \tag{4.10}$$

shows that $\tilde{\alpha} = 0$ in the case (3.17); as shown below, this case yields an additional point symmetry and an additional conservation law.

Remark 4.2. Both the PDEs (4.8) and the general system (4.3) can be further invertibly transformed into a one-parameter family of PDE systems:

$$\begin{aligned} &H_{tt} = KH_{xx} + \left(\left[3H_x^2 + G_x^2\right]H_{xx} + 2G_xH_xG_x\right), \\ &G_{tt} = KG_x + \left(2G_xH_xH_{xx} + \left(H_x^2 + 3G_x^2\right)G_x\right), \\ &K = 0, \pm 1. \end{aligned} \tag{4.11}$$

In particular, the PDEs (4.8) with $\alpha, \beta > 0$ are transformed into (4.11) with $K = 1$ by a scaling transformation

$$x = Lx^*, \quad t = L\alpha^{-1/2}t^*, \quad G = L\left(\frac{\alpha}{\beta}\right)^{1/2}G^*, \quad H = L\left(\frac{\alpha}{\beta}\right)^{1/2}H^*, \tag{4.12}$$

$L = \text{const} > 0$, and a subsequent omission of the asterisks.

The general family (4.3) is first transformed into the system (4.8) (see Remark 4.1), where one could have $\alpha > 0$, $\alpha = 0$, or $\alpha < 0$. In the case $\alpha > 0$, the transformation (4.12) is used, and the system is mapped into (4.11) with $K = 1$. If $\alpha < 0$,

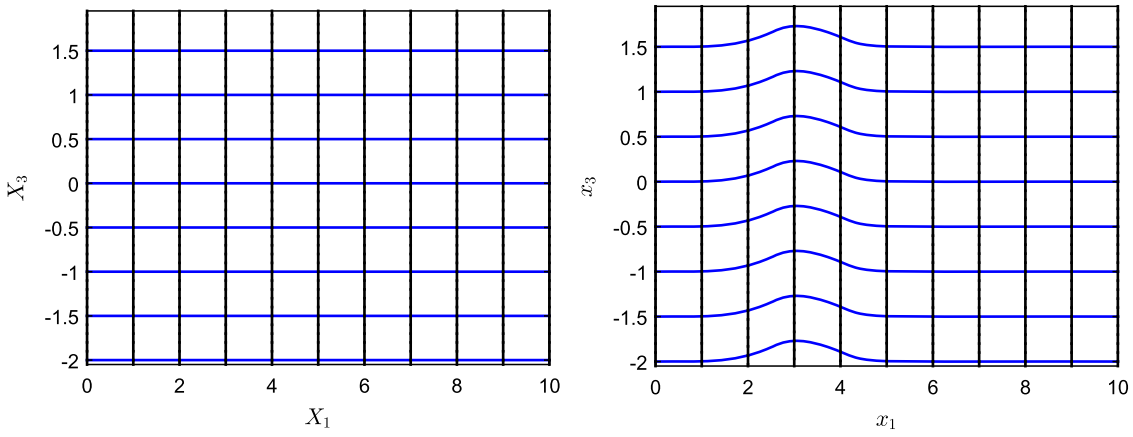

Fig. 3 – Material lines $X^1 = \text{const}$ (vertical) and the fiber lines $X^3 = \text{const}$ (blue, horizontal) for the one-dimensional hyperelastic anti-plane shear model (3.8) (fiber angle $\gamma = 0$), with physical parameters (3.30), and the Gaussian initial condition for the time $t = 1.82 \cdot 10^{-3}$ s (the corresponding dimensionless time is $\hat{t} = 3$). The material configuration (left) and the actual configuration (right). Spatial coordinates are dimensional, given in millimeters. (For interpretation of the references to color in this figure caption, the reader is referred to the web version of this paper.)

the transformation

$$t = L(-\alpha)^{-1/2}t^*, \quad G = L\left(\frac{-\alpha}{\beta}\right)^{1/2} G^*, \quad H = L\left(\frac{-\alpha}{\beta}\right)^{1/2} H^*. \tag{4.13}$$

maps the system into (4.11) with $K = -1$. Finally, when $\alpha = 0$, one takes

$$t = L\beta^{-1/2}t^*, \quad G = LG^*, \quad H = LH^*. \tag{4.14}$$

and upon the omission of asterisks, obtains the Eq. (4.11) with $K=0$.

4.1. *Conservation laws of the planar shear equations (4.11)*

As per Remark 4.2, to study the local conservation laws of the models (4.3) and (4.8), it is sufficient to classify the local conservation laws of the simplified system (4.11) with respect to the single discrete parameter K. The direct method is employed. Since the system (4.11) is in the Kovalevskaya form with respect to time, one may assume, without loss of generality, that neither the multipliers, nor the density, nor the fluxes of the conservation laws depend on H_{tt}, G_{tt} and their derivatives. In order to compute the complete set of second-order local conservation law multipliers, the latter are assumed to have the dependency:

$$\Lambda_i = \Lambda_i(x, t, H, G, H_x, G_x, H_t, G_t, H_{xx}, G_{xx}, H_{xt}, G_{xt}), \quad i = 1, 2. \tag{4.15}$$

The system of multiplier determining equations consists of 213 linear PDEs, and is solved to yield the following two cases:

Case 1: $K \neq 0$. In this case, one has seven linearly independent conservation laws, as follows:

1. The local conservation laws for Eulerian linear momenta in X^2 and X^3 directions arise for multiplier pairs $(\Lambda_1, \Lambda_2) = (1, 0)$ and $(0, 1)$. This yields the divergence forms of the momentum equation (4.2):
$$D_t\left(H_t\right) - D_x\left(\left(K + G_x^2 + H_x^2\right)H_x\right) = 0, \tag{4.16}$$
$$D_t\left(G_t\right) - D_x\left(\left(K + G_x^2 + H_x^2\right)G_x\right) = 0. \tag{4.17}$$
The global conserved quantities are the total linear momenta, given by (3.21) and the corresponding expression involving the amplitude H.
2. The conservation of the momentum in the Lagrangian frame, which is a conservation law independent of the Eulerian momenta, corresponds to the multiplier pair $(\Lambda_1, \Lambda_2) = (H_x, G_x)$ and the Lagrangian spatial translation symmetry $\partial/\partial x$. It is given by
$$D_t(H_xH_t + G_xG_t) - D_x\left(\tfrac{1}{2}\left(H_t^2 + G_t^2 + K(H_x^2 + G_x^2)\right) + \tfrac{3}{4}(H_x^2 + G_x^2)^2\right) = 0. \tag{4.18}$$
We note the difference in the factor $\frac{3}{4}$ vs. $\frac{1}{4}$ here and in the anti-plane shear case (3.22); the difference is due to the factor of 3 difference in the choice of equivalence transformations (4.12) and (3.10).
3. The local conservation of energy:
$$D_t\left(\tfrac{1}{2}\left(H_t^2 + G_t^2 + K(H_x^2 + G_x^2)\right) + \tfrac{1}{4}(H_x^2 + G_x^2)^2\right) - D_x\left(G_tG_x\left(\tfrac{1}{3}G_x^2 + K\right)\right) = 0 \tag{4.19}$$
arises from the multiplier pair $(\Lambda_1, \Lambda_2) = (H_t, G_t)$, or from Noether's theorem for the variational time-translation symmetry $\partial/\partial t$. The total energy is given by the spatial integral of the conserved density in (4.19) over the domain where the perturbation $H^2 + G^2 > 0$.
4. Two local conservation laws following from the multiplier pairs $(\Lambda_1, \Lambda_2) = (t, 0)$ and $(0, t)$, the "center of mass theorem" components in the direction of X^2 and X^3, are given by
$$D_t\left(H - tH_t\right) + D_x\left(tH_x\left(H_x^2 + G_x^2 + K\right)\right) = 0, \tag{4.20}$$
$$D_t\left(G - tG_t\right) + D_x\left(tG_x\left(H_x^2 + G_x^2 + K\right)\right) = 0. \tag{4.21}$$
The corresponding global conserved quantities describe the rates of change of the average displacement in each direction (cf. (3.24)).
5. Finally, the multiplier pair $(\Lambda_1, \Lambda_2) = (-G, H)$ corresponds to the rotation symmetry $-G\partial/\partial H + H\partial/\partial G$ in the

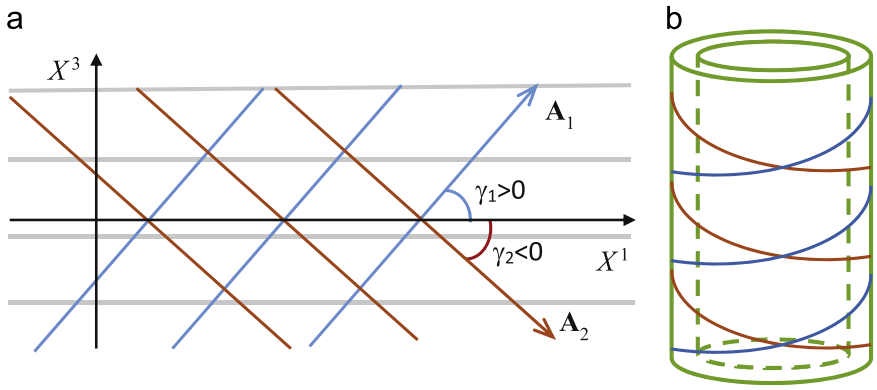

Fig. 4 – (a) Fiber directions. (b) Arterial wall (adventitia or media) setup with two helical fiber families (cf. Holzapfel et al., 2000).

(x^1, x^2)-plane, and expresses the conservation of the Eulerian angular momentum in the x^3-direction. It is given by

$$\mathrm{D_t}\big(HG_t - GH_t\big) - \mathrm{D_x}\big((HG_x - GH_x)\big(H_x^2 + G_x^2 + K\big)\big) = 0. \tag{4.22}$$

The conserved density $\Theta = HG_t - GH_t$ is the linear density of angular momentum in the material direction $x = X^1$. The global conserved quantity is the total Eulerian angular momentum of a material slab orthogonal to the axis of $x = X^1$, for $a \le x \le b$:

$$\mathcal{A} = \int_a^b (HG_t - GH_t)\, dx = \text{const.}$$

Case 2: $K=0$. In this case, one obtains an additional multiplier pair $(\Lambda_1, \Lambda_2) = (H - 3xH_x - 5tH_t, G - 3xG_x - 5tG_t)$, which clearly corresponds to the evolutionary form of the scaling symmetry:

$$\mathrm{Y} = 3x\frac{\partial}{\partial x} + 5t\frac{\partial}{\partial t} + G\frac{\partial}{\partial G} + H\frac{\partial}{\partial H}. \tag{4.23}$$

The additional local conservation law is given by the divergence expression

$$\mathrm{D_t}\Theta + \mathrm{D_x}\,\Psi = 0, \tag{4.24}$$

with the conserved density

$$\Theta = HH_t + GG_t - 3x(H_tH_x + G_tG_x) - \tfrac{5}{4}t\big(2(H_t^2 + G_t^2) + (H_x^2 + G_x^2)^2\big),$$

and the flux

$$\Psi = \tfrac{3}{2}x\big((H_t^2 + G_t^2) + 3(H_x^2 + G_x^2)^2\big) + (5t(H_tH_x + G_tG_x) - (HH_x + GG_x))\big(H_x^2 + G_x^2\big).$$

It is challenging to provide an immediate physical interpretation of the conservation law (4.24); we note that it is evidently a generalization of the anti-plane shear conservation law (3.28) (Section 3.2) onto the case $H \neq 0$.

Remark 4.3. For the planar shear model (4.3), the infinite set of first-order conservation laws does not arise for the multiplier ansatz (4.15), as it does for the anti-plane shear model (Section 3.2). Respectively, no analog of the linearizing Legendre transformation exists for the model (4.3); this is a result of essential coupling between the two nonlinear wave equations. It remains an open problem to seek conservation laws of the PDE system (4.3) arising from higher-order multipliers.

Remark 4.4. In Cheviakov et al. (2015), Lie point symmetries of the PDE model (4.8) ($\gamma = 0$) have been computed, and a family of traveling wave-type exact solutions has been derived. With the help of the invertible transformations (4.12), these results directly carry over to the planar shear model (4.3) for an arbitrary fiber angle $\gamma \in (0, \pi/2)$.

5. A two-fiber anti-plane shear model

We now generalize the model of Section 3 onto a more practically realistic case of two fiber families. We suppose that the fibers in the material configuration are straight, parallel respectively to the unit vectors

$$\mathbf{A}_1 = \begin{bmatrix} \cos\gamma_1 \\ 0 \\ \sin\gamma_1 \end{bmatrix}, \quad \mathbf{A}_2 = \begin{bmatrix} \cos\gamma_2 \\ 0 \\ \sin\gamma_2 \end{bmatrix} \tag{5.1}$$

in the (X^1, X^3)-plane. The configuration is shown in Fig. 4(a). It can be viewed as an "flat cylinder" approximation of an arterial wall setup (Holzapfel et al., 2000) with no displacements in the radial direction, and when displacements are small compared to the radius of curvature (Fig. 4(b)).

Consider a specific form of the strain energy density (cf. (2.6) and (2.8)) given by

$$W = a(I_1 - 3) + b(I_2 - 3) + q_1(I_4 - 1)^2 + q_2(I_6 - 1)^2 + K_3I_8^2 + K_4I_8, \tag{5.2}$$

We assume

$$\gamma_1 \in \Big(0, \frac{\pi}{2}\Big), \quad \gamma_2 \in \Big(-\frac{\pi}{2}, 0\Big);$$

in particular, for arterial wall models, it is common to take

$$\gamma_2 = -\gamma_1, \quad q_2 = q_1, \tag{5.3}$$

which we do not generally assume.

The model (5.2) involves six positive constant material parameters: $a, b, q_{1,2}, K_{3,4}$. As before, a, b are Mooney–Rivlin constants, $q_{1,2}$ represent the strengths of fiber effects for the two fiber families (5.1), and $K_{3,4}$ are fiber interaction constants (Peng et al., 2010). The model (5.2) is rather general in the sense that it contains first Taylor terms of the dependence of the

strain energy density W on the invariants I_1, I_2, I_4, I_6, and I_8 for a wide class of two-fiber hyperelastic constitutive models.

We are interested in deriving a nonlinear wave equation for the anti-plane shear displacement in the ansatz (3.2), naturally compatible with the incompressibility condition. This PDE will generalize the Eq. (3.6).

Upon the substitution of (5.2) and (3.2) into the dynamic equation (2.12) with no forcing, it is found that the momentum equation in the direction of X^1 can be integrated and explicitly yields the hydrostatic pressure

$$\begin{aligned} p &= 2\rho_0\kappa_1 \cos\gamma_1 \cos\gamma_2 \cos^2\big(\gamma_1-\gamma_2\big)\big(\cos\gamma_1\cos\gamma_2 G_x + \sin(\gamma_1+\gamma_2)\big)G_x \\ &\quad + \sum_{i=1}^{2}\rho_0\beta_i\cos^3\gamma_i\big(\cos\gamma_i G_x + 2\sin\gamma_i\big)G_x + f(t) \\ &= M_2 G_x^2 + M_1 G_x + f(t), \quad M_{1,2} = M_{1,2}(\kappa_1,\beta_{1,2},\gamma_{1,2}) = \text{const}, \end{aligned} \tag{5.4}$$

where the notation

$$\begin{aligned} &X^1 = x, \quad G = G(x,t), \quad p = p(x,t), \quad \alpha = 2(a+b)/\rho_0 > 0, \\ &\beta_{1,2} = 4\,q_{1,2}/\rho_0 > 0, \quad \kappa_1 = 2K_3/\rho_0 > 0, \quad \kappa_2 = 2K_4/\rho_0 > 0, \end{aligned} \tag{5.5}$$

similar to (3.4), has been adopted. The X^2-component of the momentum equation vanishes, and the X^3-component yields the wave nonlinear equation

$$G_{tt} = (AG_x^2 + BG_x + C)G_{xx}, \tag{5.6}$$

where the constants A, B, and C depend on the material parameters as follows:

$$\begin{aligned} A &= 6\kappa_1\cos^2(\gamma_1-\gamma_2)\cos^2\gamma_1\cos^2\gamma_2 + 3\sum_{i=1}^{2}\beta_i\cos^4\gamma_i > 0, \\ B &= 6\kappa_1\cos^2(\gamma_1-\gamma_2)\sin(\gamma_1+\gamma_2)\cos\gamma_1\cos\gamma_2 + 6\sum_{i=1}^{2}\beta_i\sin\gamma_i\cos^3\gamma_i, \\ C &= \kappa_1\cos^2(\gamma_1-\gamma_2)\big(\sin 2\gamma_1\sin 2\gamma_2 + \cos^2\gamma_1 + \cos^2\gamma_2\big) \\ &\quad + \kappa_2\cos(\gamma_1-\gamma_2)\cos\gamma_1\cos\gamma_2 + \sum_{i=1}^{2}\frac{\beta_i}{2}\sin^2 2\gamma_i + \alpha. \end{aligned} \tag{5.7}$$

Depending on the sign of the discriminant $D = B^2 - 4AC$, the loss of hyperbolicity in the PDE (5.6) may be possible. In particular, if $D<0$, Eq. (5.6) is always hyperbolic, and can be mapped into the familiar equation (3.18) with $K=1$. When $D>0$, the PDE is equivalent to Eq. (3.18) with $K=-1$. In both cases, the transformation is given by

$$x = L\hat{x}, \quad t = 2L\hat{t}\sqrt{\frac{A}{|D|}}, \quad G(x,t) = \sqrt{|D|}\,\frac{L}{2A}\hat{G}(\hat{x},\hat{t}) - \frac{B}{2A}x. \tag{5.8}$$

When $D=0$, Eq. (5.6) is equivalent to (3.18) with $K=0$.

Due to the equivalence of the two-fiber anti-plane shear model (5.6) to the nonlinear wave Eq. (3.18) for some fixed K, the conservation law classification repeats that of Section 3.2. Similarly, for numerical simulation, it is sufficient to perform computations for (3.18) and use the transformations inverse to (5.8) to obtain the results for the two-fiber model (5.6). The Lagrangian density for the PDEs (5.6) is also obtained from the K-family Lagrangian (3.19) through transformations inverse to (5.8).

We now present a numerical illustration of an anti-plane shear wave propagating in a material described by the constitutive model (5.2). We take the numerical parameters corresponding to the rabbit carotid artery media (Holzapfel et al., 2000), given by (3.30), with fiber angles

$$\gamma_1 = -\gamma_2 \simeq \pi/6,$$

and sample anisotropy parameters

$$\kappa_1 = 5\ \text{m}^2/\text{s}^2, \quad \kappa_2 = 0.$$

The corresponding constants A, B, and C in the wave equation (5.6) are given by

$$A \simeq 18.70\ \text{m}^2/\text{s}^2, \quad B = 0, \quad C \simeq 6.88\ \text{m}^2/\text{s}^2,$$

and the discriminant $D = B^2 - 4AC < 0$. Fig. 5 shows the material lines $X^1 = \text{const}$, $X^3 = \text{const}$ and the fiber lines $X^3 - X^1\tan\gamma_i = \text{const}, i = 1, 2$, in the Lagrangian and Eulerian configurations, for the initial conditions given by $G(x,0) = G_0\exp(-(kx)^2)$, $G_0 = 1/k = 1$ mm, with $G_t(x,0) = 0$. The d'Alembert-like solution is symmetric with respect to the X^3-axis.

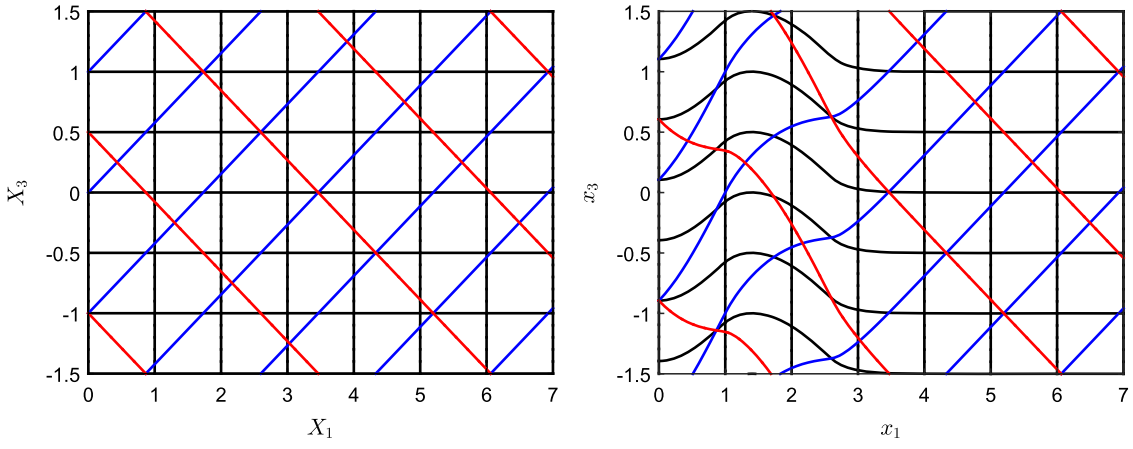

Fig. 5 – Material lines $X^1 = \text{const}$, $X^3 = \text{const}$ (black, vertical and horizontal) and the fiber lines $X^3 - X^1\tan\gamma_i = \text{const}$, $i=1, 2$ (blue, red) for the one-dimensional hyperelastic two-fiber anti-plane shear model (5.2). The material configuration (left) and the actual configuration (right) at the time $t = 5\cdot 10^{-4}$ s. Spatial coordinates are given in millimeters. (For interpretation of the references to color in this figure caption, the reader is referred to the web version of this paper.)

6. A one-dimensional hyper-viscoelastic model

The anti-plane shear model of Section 3 is now generalized to include viscoelastic effects through the use of the pseudo-invariants J_2 and J_9 defined in (2.15) and (2.17). We assume the displacements in the X^3-direction, of the form (3.2), propagating in the X^1-direction ($X^1 \equiv x$), and a single fiber family directed along the vector (3.3). The pseudo-strain energy density is given by

$$W = W^h + W^v = a(I_1-3) + b(I_2-3) + q(I_4-1)^2 + \frac{H_1}{4} J_2(I_1-3) + \frac{H_2}{2} J_9(I_4-1)^2. \tag{6.1}$$

The model involves five constant constitutive parameters. Due to the presence of the components of the tensor $\dot{\mathbf{C}}$, the forms of the PDEs resulting from the substitution of (6.1) into the equations of motion (2.12) (with no forcing) are significantly more complicated than that for the purely hyperelastic case.

We again use the short-hand notation (3.4), additionally denoting

$$\eta = H_1/\rho_0, \quad \zeta = H_2/\rho_0.$$

The physical dimension units of the coefficients η, ζ are the units of the kinematic viscosity of a viscous fluid (m^2/s). For displacements of the form (3.2), the incompressibility condition $J = \det \mathbf{F} = 1$ is identically satisfied, and the X^2-component of the momentum equation vanishes identically.

For the general form of W in (6.1), the hydrostatic pressure expression and the PDE for $G(x,t)$ can be derived from the X^1- and X^3-components of the momentum equation; their forms, however, are given by rather complicated expressions. We consider a special case of interest corresponding to the wave propagation in the fiber direction, i.e., $\gamma = 0$. In this case, the hydrostatic pressure and the PDE for the displacement are respectively given by

$$p = \rho_0\left[\beta G_x^2 + 2(\eta + 2\zeta G_x^2) G_x^3 G_{tx}\right] + f(t), \tag{6.2}$$

$$\begin{aligned} G_{tt} &= (\alpha + 3\beta G_x^2) G_{xx} \\ &\quad + \eta G_x\left(2(4G_x^2+1) G_{xx} G_{tx} + (2G_x^2+1) G_x G_{txx}\right) \\ &\quad + \zeta G_x^3\left(4(6G_x^2+1) G_{xx} G_{tx} + (4G_x^2+1) G_x G_{txx}\right). \end{aligned} \tag{6.3}$$

When $\eta = \zeta = 0$, Eqs. (6.2) and (6.3) reduce to the formulas (3.8) and (3.9) for the hyperelasticity model. We note that the damping η- and ζ-terms in (6.3) are significantly more complicated than, for example, a basic friction forcing term $-\eta G_t$ in a linear wave model describing small oscillations of an elastic string in a viscous medium.

The equivalence transformation (3.10) with some $L = \text{const}$ can be used to map the PDE (6.3) into a dimensionless form

$$\begin{aligned} \hat{G}_{\hat{t}\hat{t}} &= \left(\hat{G}_{\hat{x}}^2 + 1\right) \hat{G}_{\hat{x}\hat{x}} \\ &\quad + \hat{\eta} \hat{G}_{\hat{x}}\left[2(4\hat{\alpha}\hat{G}_{\hat{x}}^2 + 3)\hat{G}_{\hat{x}\hat{x}}\hat{G}_{\hat{t}\hat{x}} + (2\hat{\alpha}\hat{G}_{\hat{x}}^2 + 3)\hat{G}_{\hat{x}}\hat{G}_{\hat{t}\hat{x}\hat{x}}\right] \\ &\quad + \hat{\zeta}\hat{G}_{\hat{x}}^3\left[12(2\hat{\alpha}\hat{G}_{\hat{x}}^2 + 1)\hat{G}_{\hat{x}\hat{x}}\hat{G}_{\hat{t}\hat{x}} + (4\hat{\alpha}\hat{G}_{\hat{x}}^2 + 3)\hat{G}_{\hat{x}}\hat{G}_{\hat{t}\hat{x}\hat{x}}\right], \end{aligned} \tag{6.4}$$

involving the dimensionless parameters

$$\hat{\alpha} = \frac{\alpha}{\beta}, \quad \hat{\eta} = \frac{\eta\sqrt{\alpha}}{9L\beta}, \quad \hat{\zeta} = \frac{\zeta\alpha^{3/2}}{27L\beta^2}. \tag{6.5}$$

6.1. Conservation laws and potential systems of the hyper-viscoelastic fiber-aligned wave propagation model (6.4)

We now use the direct conservation law construction method (Appendix A) with third-order multipliers to seek local conservation laws of the dimensionless nonlinear PDE (6.4). For the simplicity of notation, hats on the dimensionless variables $\hat{x}, \hat{t}, \hat{G}$ will be omitted. Let the conservation law multipliers have the form

$$\Lambda = \Lambda(x, t, G, G_t, G_t, G_{xx}, G_{xt}, G_{xxx}, G_{xxt}).$$

In the general case, for arbitrary $\hat{\alpha}, \hat{\eta}, \hat{\zeta}$, two local conservation laws arise:

1. The conservation law for the multiplier $\Lambda_1 = 1$ is given by

$$D_t\left(G_t - \left[\hat{\eta}(3 + 2\hat{\alpha}G_x^2) + \hat{\zeta}(3 + 4\hat{\alpha}G_x^2)G_x^2\right]G_x^2 G_{xx}\right) - D_x\left(\left[1 + \tfrac{1}{3}G_x^2\right]G_x\right) = 0. \tag{6.6}$$

2. The conservation law for the multiplier $\Lambda_2 = t$ is given by

$$\begin{aligned} &D_t\left(tG_t - G - t\left[\hat{\eta}(3 + 2\hat{\alpha}G_x^2) + \zeta(3 + 4\hat{\alpha}G_x^2)G_x^2\right]G_x^2 G_{xx}\right) \\ &\quad + D_x\left(\hat{\eta}\left[1 + \tfrac{2}{5}\hat{\alpha}G_x^2\right]G_x^3 + \hat{\zeta}\left[\tfrac{3}{5} + \tfrac{4}{7}\hat{\alpha}G_x^2\right]G_x^5 - t\left[1 + \tfrac{1}{3}G_x^2\right]G_x\right) = 0. \end{aligned} \tag{6.7}$$

An immediate application of the conservation laws (6.6) and (6.7) is the construction of potential systems which allows for a simpler finite-difference numerical solution than the original PDE (6.4). Indeed, in the third-order PDE (6.4), derivatives involving time of the form G_{tt}, G_{tx}, and G_{txx} occur linearly. In order to solve this PDE "as is", specialized explicit finite-difference schemes can be derived. For a simpler numerical solution, one can use, for example, the conservation law (6.6) to introduce a potential variable $V(x,t)$ (cf. Bluman et al., 2010) so that the pair (G,V) satisfies the potential system

$$\begin{aligned} V_x &= G_t - \left[\hat{\eta}(3 + 2\hat{\alpha}G_x^2) + \hat{\zeta}(3 + 4\hat{\alpha}G_x^2)G_x^2\right]G_x^2 G_{xx}, \\ V_t &= \left[1 + \tfrac{1}{3}G_x^2\right]G_x. \end{aligned} \tag{6.8}$$

One consequently obtains a coupled system of evolution equations

$$\frac{\partial}{\partial t}\begin{bmatrix} G \\ V \end{bmatrix} = \begin{bmatrix} V_x + \left[\hat{\eta}(3 + 2\hat{\alpha}G_x^2) + \hat{\zeta}(3 + 4\hat{\alpha}G_x^2)G_x^2\right]G_x^2 G_{xx} \\ \left[1 + \tfrac{1}{3}G_x^2\right]G_x \end{bmatrix} \tag{6.9}$$

involving the time derivatives only in the left-hand sides. The system (6.9) can be used, for example, for numerical computations that employ a higher-order Runge–Kutta-based method of lines.

The second potential system arising from the local conservation law (6.7) is given by

$$\begin{aligned} W_x &= tG_t - G - t\left[\hat{\eta}(3 + 2\hat{\alpha}G_x^2) + \zeta(3 + 4\hat{\alpha}G_x^2)G_x^2\right]G_x^2 G_{xx}, \\ W_t &= -\left(\hat{\eta}\left[1 + \tfrac{2}{5}\hat{\alpha}G_x^2\right]G_x^3 + \hat{\zeta}\left[\tfrac{3}{5} + \tfrac{4}{7}\hat{\alpha}G_x^2\right]G_x^5 - t\left[1 + \tfrac{1}{3}G_x^2\right]G_x\right), \end{aligned} \tag{6.10}$$

and involves a nonlocal variable $W(x,t)$.

6.2. A sample numerical computation

We now numerically solve the dimensionless PDE (6.4) with the same initial data and constants as used in Section 3.3 for the dimensionless inviscid model. The finite-difference method of lines implemented in `Matlab` is applied to the potential system (6.9). The initial condition for the potential $V(x,t)$ corresponding to (3.29) is given by $V(x,0)=0$. The parameters (6.5) corresponding to the choice (3.30) with $\eta=10\ \mathrm{m}^2/\mathrm{s}$, $\zeta=5\ \mathrm{m}^2/\mathrm{s}$ are given by $\hat{\alpha}=0.636$, $\hat{\eta}=0.427$, $\hat{\zeta}=0.0453$.

Similar to the case of Section 3.3, the problem is solved in $-30\le x\le 30$ with homogeneous Dirichlet boundary conditions. The results, in comparison to those with zero viscosity (Fig. 2), are presented in Fig. 6. In addition to the evident decrease of the wave amplitude with time, for the viscoelastic case, we observe an increased stability of the computation due to the absence of wave breaking.

7. Discussion

Wave methods are widely used for the measurement of mechanical properties of biomembranes in a non-destructive manner. This involves the solution of complicated nonlinear boundary value problems. Mathematical formulation of the related basic nonlinear wave propagation models and the analysis of their structure and solution properties are therefore of high practical relevance.

In contrast to the commonly adopted incremental framework based on linear approximations of the field equations, the current contribution considered fully nonlinear time-dependent elasticity and viscoelasticity equations. Several PDE models have been presented, describing the dynamics of the following displacements in fiber-reinforced incompressible hyperelastic media:

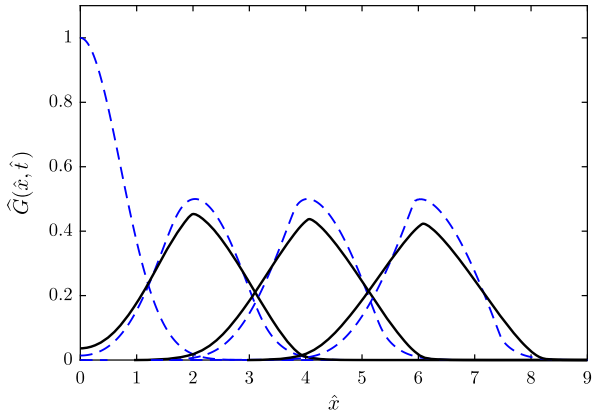

Fig. 6 – Right-traveling wave profiles for the hyper-viscoelastic fiber-aligned anti-plane shear wave propagation model (6.4) with initial conditions (3.29) (black solid curves) compared to the same initial value problem for the case of zero viscosity (dimensionless PDE (3.18) with $K=1$, blue dashed curves), for the dimensionless times $\hat{t}=0,2,4,6$ (left to right). (For interpretation of the references to color in this figure caption, the reader is referred to the web version of this paper.)

- Anti-plane shear displacements, hyperelastic model, single fiber family, and general fiber family orientation.
- Planar shear displacements perpendicular to the wave propagation direction, hyperelastic model, single fiber family, and general fiber family orientation.
- Anti-plane shear displacements, hyperelastic model, two fiber families, and general fiber family orientations.
- Anti-plane shear displacements, single fiber family, and hyper-viscoelastic framework.

Equivalence transformations were derived to substantially reduce the number of parameters in the models. In particular, it was shown that the nonlinear wave equations, arising in Sections 3 and 5, can be invertibly mapped to a nonlinear wave equation (3.18) involving a single parameter $K=0,\pm 1$.

Local conservation laws of the models were systematically constructed using the direct construction method. It was shown that the basic nonlinear PDE (3.18) admits an infinite number of conservation laws, and can be invertibly mapped into a linear variable-coefficient wave equation (3.26).

Other analytical properties of the presented models have been considered, and sample numerical solutions have been obtained. The numerical examples of Sections 3.3 and 5, even though provided mostly for illustration purposes in rather idealized settings, are based on real experimental data. The numerical solutions describe finite perturbations, thereby going significantly beyond the usual laboratory testing capabilities. Predictions of numerical simulations similar to the presented ones can be used to evaluate physical parameters, such as mechanical moduli, from an inverse approach based on a comparison with real dynamical measurements.

Future work directions will include the application of the obtained results, in particular, the local conservation laws, to analytical and numerical computations for biomembranes and other tissues and materials of interest for applications. Work will continue to extend the presented analysis to models in other geometries, including cylindrical coordinates and axial symmetry, spherical coordinates, pertinent to specific biological contexts, such as artery and cornea models (cf. Holzapfel et al., 2000; Pandolfi and Manganiello, 2006). It is also of interest and importance to generalize the presented analysis to include more general constitutive relations, ideally, constitutive relations involving arbitrary functions.

An important question related to one-dimensional reductions considered in this paper is their stability in the sense of the full three-dimensional model, in particular, the possibility of nonlinear mode interaction in three-dimensional mechanics.

Acknowledgments

A.C. is grateful to NSERC of Canada for research support through a Discovery Grant.

Appendix A. Direct construction of conservation laws

Consider a system of N partial differential equations

$$R^{\sigma}=0,\quad \sigma=1,\dots,N, \tag{A.1}$$

with m dependent variables $\mathbf{u}(t,\mathbf{x})=(u^1,\ldots,u^m)$, and independent variables t, $\mathbf{x}=(x^1,\ldots,x^n)$. The direct conservation law construction method is based on finding linear combinations of the given equations with some multipliers $\Lambda_\sigma=\Lambda_\sigma[\mathbf{u}]$, leading to divergence expressions

$$\Lambda_\sigma R^\sigma \equiv D_t\Theta + D_i\Phi^i. \tag{A.2}$$

Multipliers can depend on dependent and independent variables $t,\mathbf{x}$, $\mathbf{u}$, and prescribed partial derivatives of $\mathbf{u}$, to a fixed order. (In practice, multipliers are assumed to depend on derivatives of $\mathbf{u}$ up to some chosen prescribed order $k\geq 0$.) Then on solutions $R^\sigma=0$, a local conservation law (1.1) holds.

A differential function $F[\mathbf{u}]$ is a divergence expression if and only if it is annihilated by Euler differential operators E_{u^i} with respect to each scalar dependent variable u^i, $i=1,\ldots,m$ (Anco and Bluman, 1997; Olver, 2000; Bluman et al., 2010). The conservation law multipliers are consequently found as solutions of the linear *determining equations*:

$$E_{u^i}[\Lambda_\sigma R^\sigma]=0,\quad i=1,\ldots,m, \tag{A.3}$$

holding for *arbitrary functions* $\mathbf{u}(t,\mathbf{x})$, i.e., off of the solution space of the given system (A.1) (see, e.g., Bluman et al., 2010).

Having computed the multipliers, one proceeds to finding the conservation law density and fluxes (Cheviakov, 2010b). Specialized symbolic software is often used in conservation law (multiplier and density/flux) computations (e.g., Cheviakov, 2007).

The direct construction method is known to be complete, i.e., to yield all nontrivial conservation laws of the model up to a prescribed order, when the equations are written in the standard, general, or extended Kovalevskaya form with respect to some independent variable (Olver, 2000; Alonso, 1979).

REFERENCES

Abramowitch, S.D., Woo, S.L.-Y., 2004. An improved method to analyze the stress relaxation of ligaments following a finite ramp time based on the quasi-linear viscoelastic theory. J. Biomech. Eng. 126 (1), 92–97.

Alonso, L.M., 1979. On the Noether map. Lett. Math. Phys. 3 (5), 419–424.

Anco, S., Bluman, G., 1997. Direct construction of conservation laws from field equations. Phys. Rev. Lett. 78 (15), 2869.

Anco, S., Bluman, G., Wolf, T., 2008. Invertible mappings of nonlinear PDEs to linear PDEs through admitted conservation laws. Acta Appl. Math. 101 (1), 21–38.

Arumugam, V., Naresh, M., Sanjeevi, R., 1994. Effect of strain rate on the fracture behaviour of skin. J. Biosci. 19 (3), 307–313.

Assidi, M., Dos Reis, F., Ganghoffer, J.-F., 2011. Equivalent mechanical properties of biological membranes from lattice homogenization. J. Mech. Behav. Biomed. Mater. 4 (8), 1833–1845.

Badir, S., Mazza, E., Zimmermann, R., Bajka, M., 2013. Cervical softening occurs early in pregnancy: characterization of cervical stiffness in 100 healthy women using the aspiration technique. Prenat. Diagn. 33 (8), 737–741.

Basciano, C., Kleinstreuer, C., 2009. Invariant-based anisotropic constitutive models of the healthy and aneurysmal abdominal aortic wall. J. Biomech. Eng. 131, 021009.

Bataille, J., Kestin, J., 1979. Irreversible processes and physical interpretation of rational thermodynamics. J. Non-Equilib. Thermodyn. 4 (4), 229–258.

Benjamin, T., 1972. The stability of solitary waves. Proc. R. Soc. Lond. A. Math. Phys. Sci. 328 (1573), 153–183.

Bercoff, J., Chaffai, S., Tanter, M., Sandrin, L., Catheline, S., Fink, M., Gennisson, J., Meunier, M., 2003. In vivo breast tumor detection using transient elastography. Ultrasound Med. Biol. 29 (10), 1387–1396.

Bercoff, J., Tanter, M., Muller, M., Fink, M., 2004. The role of viscosity in the impulse diffraction field of elastic waves induced by the acoustic radiation force. IEEE Trans. Ultrason. Ferroelectr. Freq. Control 51 (11), 1523–1536.

Bihlo, A., Cardoso-Bihlo, E.D.S., Popovych, R.O., 2012. Complete group classification of a class of nonlinear wave equations. J. Math. Phys. 53 (12), 123515.

Biot, M., 1954. Theory of stress–strain relations in anisotropic viscoelasticity and relaxation phenomena. J. Appl. Phys. 25 (11), 1385–1391.

Biot, M., 1965. In: Mechanics of Incremental Deformations. Wiley, New York.

Bluman, G., Kumei, S., 1989. Symmetry and Differential Equations, Applied Mathematical Sciences, vol. 81. Springer, New York.

Bluman, G., Cheviakov, A., Ganghoffer, J.F., 2008. Nonlocally related PDE systems for one-dimensional nonlinear elastodynamics. J. Eng. Math. 62 (3), 203–221.

Bluman, G.W., Cheviakov, A.F., Anco, S.C., 2009. Construction of conservation laws: how the direct method generalizes Noether's theorem. In: Proceedings of the Fourth Workshop in Group Analysis of Differential Equations & Integrability, pp. 1–23.

Bluman, G.W., Cheviakov, A.F., Anco, S.C., 2010. Applications of Symmetry Methods to Partial Differential Equations. Applied Mathematical Sciences, vol. 168. Springer, New York.

Boal, D.H., 2012. In: Mechanics of the Cell. Cambridge University Press, Cambridge, UK.

Boehler, J., 1978. Lois de comportement anisotrope des milieux continus. J. Méc. 17 (2), 153–190.

Boubaker, M.B., 2009. Contribution mécanique à la réduction des marges en radiothérapie de la prostate: modélisation et simulation numérique du mouvement et de la déformation des organes pelviens (Ph.D. thesis). Institut National Polytechnique de Lorraine.

Boulanger, P., Hayes, M., Trimarco, C., 1994. Finite-amplitude plane waves in deformed Hadamard elastic materials. Geophys. J. Int. 118 (2), 447–458.

Budiansky, B., Rice, J., 1973. Conservation laws and energy-release rates. J. Appl. Mech. 40 (1), 201–203.

Caruthers, J.M., Adolf, D.B., Chambers, R.S., Shrikhande, P., 2004. A thermodynamically consistent, nonlinear viscoelastic approach for modeling glassy polymers. Polymer 45 (13), 4577–4597.

Catheline, S., Gennisson, J.-L., Fink, M., 2003. Measurement of elastic nonlinearity of soft solid with transient elastography. J. Acoust. Soc. Am. 114 (6), 3087–3091.

Catheline, S., Gennisson, J.-L., Delon, G., Fink, M., Sinkus, R., Abouelkaram, S., Culioli, J., 2004. Measurement of viscoelastic properties of homogeneous soft solid using transient elastography: an inverse problem approach. J. Acoust. Soc. Am. 116 (6), 3734–3741.

Checa, S., Prendergast, P.J., Duda, G.N., 2011. Inter-species investigation of the mechano-regulation of bone healing: comparison of secondary bone healing in sheep and rat. J. Biomech. 44 (7), 1237–1245.

Cheviakov, A.F., 2007. GeM software package for computation of symmetries and conservation laws of differential equations. Comput. Phys. Commun. 176 (1), 48–61.

Cheviakov, A.F., 2010a. Symbolic computation of local symmetries of nonlinear and linear partial and ordinary differential equations. Math. Comput. Sci. 4 (2–3), 203–222.

Cheviakov, A.F., 2010b. Computation of fluxes of conservation laws. J. Eng. Math. 66 (1–3), 153–173.

Cheviakov, A.F., "Symbolic Computation of Nonlocal Symmetries and Nonlocal Conservation Laws of Partial Differential Equations Using the GeM Package for Maple." In Similarity and Symmetry Methods, pp. 165-184. Springer International Publishing, 2014.

Cheviakov, A., Ganghoffer, J.F., 2012. Symmetry properties of two-dimensional Ciarlet–Mooney–Rivlin constitutive models in nonlinear elastodynamics. J. Math. Anal. Appl. 396 (2), 625–639.

Cheviakov, A., St. Jean, S., 2015. A comparison of conservation law construction approaches for the two-dimensional incompressible Mooney–Rivlin hyperelasticity model, submitted for publication.

Cheviakov, A., Ganghoffer, J.F., St. Jean, S., 2015. Fully non-linear wave models in fiber-reinforced anisotropic incompressible hyperelastic solids. Int. J. Non-Linear Mech. 71, 8–21.

Ciarlet, P.G., 1988. Mathematical Elasticity. Volume I: Three-dimensional Elasticity, Collection Studies in Mathematics and Applications, vol. 20. Elsevier, Amsterdam.

Coleman, B.D., Noll, W., 1961. Foundations of linear viscoelasticity. Rev. Mod. Phys. 33 (2), 239.

Coleman, B.D., Noll, W., 1963. The thermodynamics of elastic materials with heat conduction and viscosity. Arch. Ration. Mech. Anal. 13 (1), 167–178.

Criscione, J.C., Sacks, M.S., Hunter, W.C., 2003. Experimentally tractable, pseudo-elastic constitutive law for biomembranes: I. Theory. J. Biomech. Eng. 125 (1), 94–99.

Dafalias, Y., 1991. Constitutive model for large viscoelastic deformations of elastomeric materials. Mech. Res. Commun. 18 (1), 61–66.

De Groot, S.R., 1951. In: Thermodynamics of Irreversible Processes. North-Holland, Amsterdam.

Demirkoparan, H., Pence, T., Wineman, A., 2010. Torsion of a Fiber Reinforced Hyperelastic Cylinder for which the Fibers can Undergo Dissolution and Reassembly, vol. 48, no. 11, pp. 1179–1201.

Ehret, A.E., Itskov, M., 2007. A polyconvex hyperelastic model for fiber-reinforced materials in application to soft tissues. J. Mater. Sci. 42 (21), 8853–8863.

Fay, J., Puria, S., Decraemer, W.F., Steele, C., 2005. Three approaches for estimating the elastic modulus of the tympanic membrane. J. Biomech. 38 (9), 1807–1815.

Fung, Y.C., 1993. In: Biomechanics: Mechanical Properties of Living Tissues. Springer, New York.

Germain P., Cours de Mécanique des Milieux Continus vol. 1, 1973, Masson et Cie Laval, impr. Barnéoud.

Hah, Z., Hazard, C., Cho, Y.T., Rubens, D., Parker, K., 2010. Crawling waves from radiation force excitation. Ultrason. Imaging 32 (3), 177–189.

Hatfield, G., Olver, P.J., 1998. Canonical forms and conservation laws in linear elastostatics. Arch. Mech. 50 (3), 389–404.

Haupt, P., 1993a. In: Thermodynamics of Solids. Springer, Vienna.

Haupt, P., 1993b. On the mathematical modelling of material behavior in continuum mechanics. Acta Mech. 100 (3–4), 129–154.

Holzapfel, G.A., 2000. In: Nonlinear Solid Mechanics: A Continuum Approach for Engineering. Wiley and Sons, Chichester, England.

Holzapfel, G.A., Ogden, R.W., 2009. Constitutive modelling of passive myocardium: a structurally based framework for material characterization. Philos. Trans. R. Soc. Lond. A: Math. Phys. Eng. Sci. 367 (1902), 3445–3475.

Holzapfel, G., Gasser, T., Ogden, R., 2000. A new constitutive framework for arterial wall mechanics and a comparative study of material models. J. Elast. 61, 1–48.

Humphrey, J., 1998. Computer methods in membrane biomechanics. Comput. Methods Biomech. Biomed. Eng. 1 (3), 171–210.

Humphrey, J., 2003. Continuum biomechanics of soft biological tissues. Proc. R. Soc. Lond. Ser. A Math. Phys. Sci. 459, 3–46.

Humphrey, J., Yin, F., 1987. On constitutive relations and finite deformations of passive cardiac tissue: I. A pseudostrain-energy function. J. Biomech. Eng. 109 (4), 298–304.

Hurschler, C., Loitz-Ramage, B., Vanderby, R., 1997. A structurally based stress–stretch relationship for tendon and ligament. J. Biomech. Eng. 119 (4), 392–399.

Hutter, K., 1977. The foundations of thermodynamics, its basic postulates and implications. a review of modern thermodynamics. Acta Mech. 27 (1–4), 1–54.

Ibragimov, N., 1994. CRC Handbook of Lie Group Analyis of Differential Equations, vol. 1. CRC Press, Boca Raton.

Joyce, E.M., Moore, J.J., Sacks, M.S., 2009. Biomechanics of the fetal membrane prior to mechanical failure: review and implications. Eur. J. Obstet. Gynecol. Reprod. Biol. 144, S121–S127.

Kettaneh, A., Marcellin, P., Douvin, C., Poupon, R., Ziol, M., Beaugrand, M., De Lédinghen, V., 2007. Features associated with success rate and performance of FibroScan measurements for the diagnosis of cirrhosis in HCV patients: a prospective study of 935 patients. J. Hepatol. 46 (4), 628–634.

Knops, R., Stuart, C., 1984. Quasiconvexity and uniqueness of equilibrium solutions in nonlinear elasticity. Arch. Ration. Mech. Anal. 86 (3), 233–249.

Krouskop, T., Dougherty, D., Vinson, F., et al., 1987. A pulsed Doppler ultrasonic system for making noninvasive measurements of the mechanical properties of soft tissue. J. Rehabil. Res. Dev. 24 (2), 1–8.

Kumei, S., Bluman, G.W., 1982. When nonlinear differential equations are equivalent to linear differential equations. SIAM J. Appl. Math. 42 (5), 1157–1173.

Lax, P., 1968. Integrals of nonlinear equations of evolution and solitary waves. Commun. Pure Appl. Math. 21 (5), 467–490.

Lerner, R.M., Parker, K.J., Holen, J., Gramiak, R., Waag, R.C., 1988. Sono-elasticity: medical elasticity images derived from ultrasound signals in mechanically vibrated targets. Acoust. Imaging 16, 317–327.

Le Tallec, P., Rahier, C., Kaiss, A., 1993. Three-dimensional incompressible viscoelasticity in large strains: formulation and numerical approximation. Comput. Methods Appl. Mech. Eng. 109 (3), 233–258.

LeVeque, R., 1992. In: Numerical Methods for Conservation Laws. Birkhauser, Basel.

Levinson, S.F., Shinagawa, M., Sato, T., 1995. Sonoelastic determination of human skeletal muscle elasticity. J. Biomech. 28 (10), 1145–1154.

Li, B., Cao, Y.-P., Feng, X.-Q., Gao, H., 2011. Surface wrinkling of mucosa induced by volumetric growth: theory, simulation and experiment. J. Mech. Phys. Solids 59 (4), 758–774.

Limbert, G., Taylor, M., 2002. On the constitutive modeling of biological soft connective tissues: a general theoretical framework and explicit forms of the tensors of elasticity for strongly anisotropic continuum fiber-reinforced composites at finite strain. Int. J. Solids Struct. 39 (8), 2343–2358.

Lubliner, J., 1985. A model of rubber viscoelasticity. Mech. Res. Commun. 12 (2), 93–99.

Maher, E., Creane, A., Lally, C., Kelly, D.J., 2012. An anisotropic inelastic constitutive model to describe stress softening and permanent deformation in arterial tissue. J. Mech. Behav. Biomed. Mater. 12, 9–19.

Marchesseau, S., Heimann, T., Chatelin, S., Willinger, R., Delingette, H., 2010. Fast porous visco-hyperelastic soft tissue model for surgery simulation: application to liver surgery. Prog. Biophys. Mol. Biol. 103 (2), 185–196.

Marsden, J.E., Hughes, T.J.R., Mathematical Foundations of Elasticity. Dover Publications, Inc., New York, 1994.

Merodio, J., Goicolea, J., 2007. On thermodynamically consistent constitutive equations for fiber-reinforced nonlinearly

viscoelastic solids with application to biomechanics. Mech. Res. Commun. 34 (7), 561–571.
Merodio, J., Ogden, R.W., 2005. Mechanical response of fiber-reinforced incompressible non-linearly elastic solids. Int. J. Non-Linear Mech. 40 (2), 213–227.
Mitri, F.G., Urban, M.W., Fatemi, M., Greenleaf, J.F., 2011. Shear wave dispersion ultrasonic vibrometry for measuring prostate shear stiffness and viscosity: an in vitro pilot study. IEEE Trans. Biomed. Eng. 58 (2), 235–242.
Ogden, R.W., 2007. Incremental Statics and Dynamics of Pre-Stressed Elastic Materials, pp. 1–26.
Ogden, R.W., Holzapfel, G.A., 2006. In: Mechanics of Biological Tissue. Springer-Verlag, Berlin, Heidelberg.
Olver, P., 2000. Applications of Lie Groups to Differential Equations, vol. 107. Springer Verlag, New York.
Orescanin, M., Qayyum, M.A., Toohey, K.S., Insana, M.F., 2010. Dispersion and shear modulus measurements of porcine liver. Ultrason. Imaging 32 (4), 255–266.
Ovsiannikov, L.V., 1982. In: Group Analysis of Differential Equations. Academic Press, New York.
Palmeri, M.L., Wang, M.H., Dahl, J.J., Frinkley, K.D., Nightingale, K. R., 2008. Quantifying hepatic shear modulus in vivo using acoustic radiation force. Ultrasound Med. Biol. 34 (4), 546–558.
Pandolfi, A., Manganiello, F., 2006. A model for the human cornea: constitutive formulation and numerical analysis. Biomech. Model. Mechanobiol. 5 (4), 237–246.
Parker, K.J., Lerner, R., 1992. Sonoelasticity of organs: shear waves ring a bell. J. Ultrasound Med. 11 (8), 387–392.
Peña, J., Martínez, M., Peña, E., 2011. A formulation to model the nonlinear viscoelastic properties of the vascular tissue. Acta Mech. 217 (1–2), 63–74.
Peng, X., Guo, Z., Harrison, P., et al., 2010. A simple anisotropic fiber reinforced hyperelastic constitutive model for woven composite fabrics. Int. J. Mater. Form. 3 (1), 723–726.
Pioletti, D.P., Rakotomanana, L.R., 2000. Non-linear viscoelastic laws for soft biological tissues. Eur. J. Mech. A-Solids 19 (LBO-ARTICLE 2000-002), 749–759.
Pioletti, DominiqueP., Rakotomanana, R.L., Gilliéron, C., Leyvraz, P.F., Benvenuti, J.F., 1996. Nonlinear viscoelasticity of the ACL: Experiments and theory. Computer Methods in Biomedical and Bioengineering, 271–280.
Prevost, T.P., Balakrishnan, A., Suresh, S., Socrate, S., 2011. Biomechanics of brain tissue. Acta Biomater. 7 (1), 83–95.
Rabbah, J.P.M., Saikrishnan, N., Siefert, A.W., Santhanakrishnan, A., Yoganathan, A.P., 2013. Mechanics of healthy and functionally diseased mitral valves: a critical review. J. Biomech. Eng. 135 (2), 021007.
Reese, S., Govindjee, S., 1998. A theory of finite viscoelasticity and numerical aspects. Int. J. Solids Struct. 35 (26), 3455–3482.
Rivlin, R.S., 1947. Torsion of a rubber cylinder. J. Appl. Phys. 18, 444–449.
Roan, E., Vemaganti, K., 2011. Strain rate-dependent viscohyperelastic constitutive modeling of bovine liver tissue. Med. Biol. Eng. Comput. 49 (4), 497–506.
Rouze, N., Wang, M., Palmeri, M., Nightingale, K., 2013. Finite element modeling of impulsive excitation and shear wave propagation through in an incompressile, transversely isotropic medium. J. Biomech. 46, 2761–2768.
Roylance, D., 2001. Engineering Viscoelasticity, Department of Materials Science and Engineering-Massachusetts Institute of Technology, vol. 2139, Cambridge, MA, pp. 1–37.
Saccomandi, G., 2007. Finite amplitude waves in nonlinear elastodynamics and related theories: a personal overview, Waves in Nonlinear Pre-Stressed Materials. Springer, Vienna, 129–179.
Saccomandi, G., Vitolo, R., 2014. On the mathematical and geometrical structure of the determining equations for shear waves in nonlinear isotropic incompressible elastodynamics. J. Math. Phys. 55 (8), 081502.
Sacks, M.S., 2000. Biaxial mechanical evaluation of planar biological materials. J. Elast. Phys. Sci. Solids 61 (1–3), 199–246.
Sandrin, L., Fourquet, B., Hasuqenoph, J.M., Yon, S., Fournier, C., Mal, F., Christidis, C., Zio, M., Poulet, B., Kazemi, F., Beaugrand, M., Palau, R., 2003. Transient elastography: a new noninvasive method for assessment of hepatic fibrosis. Ultrasound Med. Biol. 29, 1705–1713.
Sarvazyan, A., Rudenko, O., Swanson, S., Fiowlkes, J., Emelianov, 1998. Shear wave elastic imaging: a new ultrasonic technique of medical diagnostics. Ultrasound Med. Biol. 24, 1419–1435.
Shergold, O.A., Fleck, N.A., Radford, D., 2006. The uniaxial stress versus strain response of pig skin and silicone rubber at low and high strain rates. Int. J. Impact Eng. 32 (9), 1384–1402.
Sidoroff, F., 1974. Un modèle viscoélastique non linéaire avec configuration intermédiaire. J. Méc. 13 (4), 679–713.
Spencer, A.J.M., 1984. In: Continuum theory of the mechanics of fibre-reinforced composites (Vol. 282, pp. 1-32). Springer, New York.
Thurston, R., 1965. Effective elastic coefficients for wave propagation in crystals under stress. J. Acoust. Soc. Am. 37 (2), 348–356.
Tokuoka, T., Saito, M., 1969. Elastic wave propagations and acoustical birefringence in stressed crystals. J. Acoust. Soc. Am. 45 (5), 1241–1246.
Toms, S.R., Dakin, G.J., Lemons, J.E., Eberhardt, A.W., 2002. Quasi-linear viscoelastic behavior of the human periodontal ligament. J. Biomech. 35 (10), 1411–1415.
Toupin, R., Bernstein, B., 1961. Sound waves in deformed perfectly elastic materials. Acoustoelastic effect. J. Acoust. Soc. Am. 33 (2), 216–225.
Truesdell, C., Noll, W., 2004. The non-linear field theories of mechanics. Springer, Berlin, Heidelberg 1–579.
Valdez, M., Balachandran, B., 2013. Longitudinal nonlinear wave propagation through soft tissue. J. Mech. Behav. Biomed. Mater. 20, 192–208.
Vappou, J., Maleke, C., Konofagou, E.E., 2009. Quantitative viscoelastic parameters measured by harmonic motion imaging. Phys. Med. Biol. 54 (11), 3579.
Yamakoshi, Y., Sato, J., Sato, T., 1990. Ultrasonic imaging of internal vibration of soft tissue under forced vibration. IEEE Trans. Ultrason. Ferroelectr. Freq. Control 37 (2), 45–53.
Yanjun, Z., Kun, H., Chuanqing, X., Jing, Z., Guangci, S., 2001. Viscoelastic characteristics of expanded skin after grafting. Acta Mech. Solida Sin. 14 (4).
Zöllner, A.M., Tepole, A.B., Kuhl, E., 2012. On the biomechanics and mechanobiology of growing skin. J. Theor. Biol. 297, 166–175.